

**CHARACTERIZATION OF A
CHROMOSOMAL DUPLICATION IN THE *PLP1* LOCUS:
A NEW MOUSE MODEL OF PELIZAEUS-MERZBACHER DISEASE**

by

Kristi Clark

A thesis submitted to the Faculty of the University of Delaware in partial fulfillment of the requirements for the degree of Master of Science in Biological Sciences

Spring 2011

Copyright 2011 Kristi Clark
All Rights Reserved

**CHARACTERIZATION OF A
CHROMOSOMAL DUPLICATION IN THE *PLP1* LOCUS:
A NEW MOUSE MODEL OF PELIZAEUS-MERZBACHER DISEASE**

by
Kristi Clark

Approved: _____
Grace M. Hobson, Ph.D.
Co-Professor in charge of thesis on behalf of the Advisory Committee

Approved: _____
Patricia A. DeLeon, Ph.D.
Co-Professor in charge of thesis on behalf of the Advisory Committee

Approved: _____
Randall L. Duncan, Ph.D.
Chair of the Department of Biological Sciences

Approved: _____
George H. Watson, Ph.D.
Dean of the College of Arts and Sciences

Approved: _____
Charles G. Riordan, Ph.D.
Vice Provost for Graduate and Professional Education

ACKNOWLEDGMENTS

I would like to thank my advisor, Dr. Grace Hobson, for allowing me to join her laboratory and work on this amazing project during my graduate studies. Thank you to Dr. Erica Selva and Dr. Patrica DeLeon for taking the time to be a part of my committee.

I would like to thank my fellow lab members for their support: Karen Sperle for much instruction and guidance, Heather Keskeny and Linda Banser for their generous help, Lauren Sakowski for her help and continuation of this project, and Stephanie Tantzer for not just being a great help in the laboratory, but also being a faithful friend.

I must also thank the Laboratory of Dr. Robert Skoff, specifically Denise Bessert, for the time you put into helping me with this project and all your instruction. I want to thank the Bio-Imaging center at University of Delaware, specifically Dr. Kirk Czymmek and Shannon Modla, for all your support and instruction.

I wish to thank my fellow SNERPs for helping me every step of the way throughout my graduate career, especially Hunter Stitik and David Wu. Without your generosity and huge hearts I would not have made it this far.

Finally to my amazing friends and family, I want to thank you for all your love and support that continually motivates me to chase my dreams.

TABLE OF CONTENTS

LIST OF TABLES.....	vi
LIST OF FIGURES	viii
ABSTRACT	ix

Chapter

1	INTRODUCTION	1
1.1	Pelizaeus-Merzbacher disease; clinical and physical phenotype.....	1
1.2	Myelination and CNS function	3
1.3	Genetics and molecular basis of disease.....	6
1.4	Animal models.....	9
1.4.1	Existing transgenic models of PMD.....	10
1.4.2	The <i>Plp1</i> dup mouse model of PMD.....	14
2	MATERIALS AND METHODS	19
2.1	Mice.....	19
2.2	Genotyping	20
2.2.1	Nucleic acid isolation and purification.....	20
2.2.2	Genotyping analysis.....	20
2.3	RNA expression.....	23
2.3.1	Nucleic acid isolation and purification.....	23
2.3.2	Semi-quantitative and real-time quantitative RT-PCR.....	24
2.4	Protein expression	27
2.4.1	Protein isolation.....	27
2.4.2	Western analysis	28

2.5	Pathology	29
2.5.1	Histology	29
2.5.2	Confocal and electron microscopy	30
2.6	X-ray analysis	32
3	RESULTS	34
3.1	Validation of duplication	34
3.2	<i>Plp1</i> dup mice have a distinct physical phenotype due to a chromosomal duplication in the <i>Plp1</i> locus that includes the entire <i>Plp1</i> gene	35
3.3	A chromosomal duplication in the <i>Plp1</i> locus that includes the entire <i>Plp1</i> gene alters expression of PLP1	37
3.3.1	The duplication alters <i>Plp1</i> mRNA expression	37
3.3.2	The duplication alters PLP1 protein expression at P12	38
3.3.3	The duplication does not alter the <i>Plp1</i> /(<i>Plp1</i> + <i>Dm20</i>) splice ratio	39
3.4	A duplication in the <i>Plp1</i> locus that includes the entire <i>Plp1</i> gene alters expression of four of the five other genes found within the duplication	39
3.5	A duplication in the <i>Plp1</i> locus that includes the entire <i>Plp1</i> gene affects expression of other myelin proteins	41
3.6	A duplication in the <i>Plp1</i> locus that includes the entire <i>Plp1</i> gene disrupts normal myelin formation	42
4	DISCUSSION	62
	APPENDIX	74
	REFERENCES	79

LIST OF TABLES

Table 1.1	Summary of phenotype and <i>Plp1</i> dosage of existing PMD transgenic rodents and the human disease.....	16
Table 2.1	Primers used for genotyping and RT-PCR	33
Table 3.1	Validation of duplication by capillary electrophoresis of multiplex PCR, analysis of gel in figure 3.1b	47

LIST OF FIGURES

Figure 1.1	Diagram of PLP1	17
Figure 1.2	Diagram summarizing targeting steps in making of the <i>Plp1</i> dup mouse	18
Figure 3.1	Validation of duplication by semi-quantitative multiplex PCR and by amplification across <i>hprt</i> gene.....	48
Figure 3.2	Weight difference in <i>Plp1</i> dup males compared to wild-type males at six months of age.....	49
Figure 3.3	X-ray analysis of the <i>Plp1</i> dup five month old male mice	50
Figure 3.4	Developmental profile of <i>Plp1+Dm20</i> mRNA expression in <i>Plp1</i> dup and wild-type mouse brain.....	51
Figure 3.5	Altered expression of <i>Plp1+Dm20</i> mRNA and PLP1+DM20 protein in <i>Plp1</i> dup relative to wild-type mice.....	52
Figure 3.6	<i>Plp1</i> and <i>Dm20</i> alternatively spliced transcript levels in the <i>Plp1</i> dup are similar to wild-type	53
Figure 3.7	Altered mRNA expression of the genes within the duplicating, other than <i>Plp1</i> , of <i>Plp1</i> dup mice relative to wild-type mice.....	54
Figure 3.8	Close to wild-type expression levels of CNPase mRNA over the developmental set with lower protein levels in adult <i>Plp1</i> dup mice compared to wild-type.....	55
Figure 3.9	Wild-type levels of MAG mRNA expression with altered protein levels in the <i>Plp1</i> dup mice compared to wild-type mice	56
Figure 3.10	Lower levels of MBP mRNA and protein expression in the <i>Plp1</i> dup mice compared to wild-type mice.....	57
Figure 3.11	Discontinuous myelination pattern in the corpus collosum of <i>Plp1</i> dup mice.....	58

Figure 3.12	Discontinuous myelination pattern in the white matter tracks of the cerebellum of <i>Plp1dup</i>	59
Figure 3.13	Disruption of normal myelin formation in <i>Plp1dup</i> spinal cord	60
Figure 3.14	Preliminary data indicating how specific regions of the brain will be mapped for electron microscopy using confocal microscopy	61

ABSTRACT

Pelizaeus-Merzbacher disease (PMD) is a rare, progressive, degenerative central nervous system disorder in which coordination, motor abilities, and intellectual function deteriorate. The disease is one of the leukodystrophies, a group of disorders that affect growth of the myelin sheath. It is caused by mutations of the proteolipid protein 1 gene (*Plp1*), which is located on the X chromosome and encodes the most abundant protein of myelin. About 50-75% of PMD cases are due to duplications of a region of the X chromosome that includes the entire *Plp1* gene. The duplications are typically in a head-to-tail arrangement and they vary in size and gene content.

Although rodent models have been developed, these models have *Plp1* gene copies that range from two to fourteen, and none contain an actual genomic rearrangement that resemble those found in PMD patients. The mouse chromosome engineering resources (MICER) were used to generate the *Plp1dup* mouse model by introducing a duplication into the mouse genome that is similar to human duplications. The X chromosome duplication is 270 kb in size, which is within the size range of human duplications, and in addition to *Plp1*, it contains five other surrounding genes that are also commonly duplicated in PMD patients. In this work, the new mouse model was characterized, and it was concluded that a duplication that includes the entire *Plp1* gene leads to a complex expression pattern of *Plp1* and not just a simple

overexpression. A duplication in the *Plp1* locus alters the expression of *Plp1* as well as four of the other five genes within the duplication. Mice with the genomic duplication also display altered expression in other important myelin proteins leading to a disruption in normal myelin formation. Our initial *Plp1*dup mice characterization studies have only begun to reveal how a duplication of the *Plp1* locus results in a disease phenotype.

Chapter 1

INTRODUCTION

1.1 Pelizaeus-Merzbacher disease; clinical and physical phenotype

Pelizaeus-Merzbacher disease (PMD) is a rare neurological disorder affecting the central nervous system (CNS) white matter. Frederick Pelizaeus described a family with severe neurological impairments as being affected by a disease that was passed on by the mother, but does not affect her directly, in 1885, long before Mendel's rules of inheritance (Pelizaeus, 1885). Ludwig Merzbacher investigated the same family 25 years later and described the widespread lack of myelin staining in the cerebral white matter observed by a pathological analysis of the brain of an affected man (Merzbacher, 1910). PMD is a disease with variable clinical and neuropathological phenotypes and is now known to be one of the leukodystrophies (Hudson, Puckett, Berndt, Chan, & Gencic, 1989). The leukodystrophies are dysmyelinating diseases that cause abnormal formation, destruction, or turnover of myelin (Cheon et al., 2002).

A wide range of symptoms and severity are observed among PMD patients. Clinical phenotypes develop early in infancy: poor head and motor control, tremors, titubation of the head and neck when infant is seated, and an involuntary eye

movement or jumping known as nystagmus (Reviewed by Garbern, 2007). The disease is slowly progressive, and the patients will begin to develop more symptoms, such as ataxia, tremor of the upper limbs, spasticity of the limbs, athetotic movements, and cognitive impairment (Reviewed by Garbern, 2007). Symptoms are most commonly present within the first year of life, but patients live for about six decades (Woodward et al., 2005).

Abnormal myelin formation throughout the brain is a distinct phenotype of PMD. A non-uniform histochemical staining of the white matter in PMD patients was observed, and areas of relatively preserved myelin staining with the lack of myelin stain in other areas gave the white matter a patchy or “tigroid” appearance (Seitelberger, 1954). An almost complete lack of normal myelination was seen in PMD patients by a T2-weighted MRI of the brain (Caro & Marks, 1990; Cheon et al., 2002). Abnormalities in myelin formation observed by MRI were described as discontinuous with preserved areas creating myelin islets (van der Knaap & Valk, 1989). MRI data confirmed the hypothesis that PMD is due to arrest of myelination during early development, and slow degradation of myelin may possibly occur later (van der Knaap & Valk, 1989).

1.2 Myelination and CNS function

The myelin sheath is an important membrane structure in nervous system that is around the majority of axons. Myelin has been shown to be important in human development, which is evident by the array of different neurological diseases with altered myelin, such as multiple sclerosis (Baumann & Pham-Dinh, 2001). The unique composition and segmental structure of the myelin sheath allows support for the fast nerve conduction within the thin axon fibers (Baumann & Pham-Dinh, 2001). Myelin completely envelopes axons except at the nodes of Ranvier, the small gaps of less than 1µm in which axons are directly exposed (Arroyo et al., 2001). The role of the myelin sheath is to create a region of high electrical resistance and facilitate saltatory conduction by reducing current flow across the internodal axonal membrane (Arroyo et al., 2001). Saltatory conduction is the transmission of action potentials along myelinated axons from one node of Ranvier to the next. This increases the conduction velocity of action potentials without needing to increase the diameter of an axon and allows the electrical impulses of the axon to travel faster than they would otherwise (Huxley & Stampfli, 1949).

Oligodendrocytes are the cells that produce the myelin that surrounds axons in the CNS. The myelin is synthesized by the extension and modification of the plasma membrane of the oligodendrocyte. A single oligodendrocyte can myelinate up to 50 axonal segments (Pfeiffer, Warrington, & Bansal, 1993). The mechanisms and exact signals that regulate the complex process of myelination are not completely

understood. The expression of major myelin proteins depends on the contact of glial cells with axons (Scherer, Vogelbacker, & Kamholz, 1992). As the oligodendrocyte cell membrane spirals around the axon, most of the cytoplasmic contents between membrane layers extrudes to form compact myelin around the internode, which serves to create a high electrical resistance. However, at the outer edges of the internodal sheath, at the paranodal loops, and the clefts of Schmidt-Lanterman are other areas where the cytoplasmic space remains enlarged (Garbern, 2007).

Myelin contains many proteins that are important in its development. Some of these proteins are used as myelin developmental markers, since immature oligodendrocytes express 2', 3' -Cyclic Nucleotide 3' -Phosphodiesterase (CNPase), and mature oligodendrocytes express Proteolipid Protein 1 (PLP1), Myelin Basic Protein (MBP), and Myelin Associated Glycoprotein (MAG) (Dubois-Dalcq, Behar, Hudson, & Lazzarini, 1986; Monge, Kadiiski, Jacque, & Zalc, 1986). PLP1 and MBP are the most abundant proteins of CNS myelin, accounting for 50% and 30% of total protein composition, respectively (Ellis & Malcolm, 1994; Hudson et al., 1989). Both PLP1 and MBP are thought to play important roles in intra- and extracellular myelin compaction. Normal development of the neuronal cytoskeleton in the CNS neurons requires the proper formation of the compact myelin sheath (Brady et al., 1999). MBP so far is the only protein found to be essential for formation of CNS myelin because without it the compact myelin is absent. It is termed the 'executive molecule of myelin' (Boggs, 2006). On the other hand, when *Plp1* is knocked out only subtle

abnormalities in the compaction of myelin was observed. Degenerating axons are the more striking pathological abnormality observed when *Plp1* is knocked out (I. Griffiths et al., 1998). The absence of PLP1 protein negatively affects the maintenance of the myelin sheath (Garbern, 2007).

PLP1 is synthesized on the rough endoplasmic reticulum (ER) and is transported through the Golgi complex where it associates with other essential parts of myelin in membrane rafts (Simons, Kramer, Thiele, Stoffel, & Trotter, 2000). Raft formation is part of the initial myelin assembly. It is followed by vesicular transport of PLP1 into the myelin membrane (Schneider et al., 2005). Mutations that cause PLP1 protein misfolding prevent correct vesicular transport through the Golgi. Instead, misfolded PLP1 triggers the unfolded protein response that induces ER associated degradation (Gow & Lazzarini, 1996; Meusser, Hirsch, Jarosch, & Sommer, 2005). However, overexpression of normal PLP1 does not trigger this unfolded protein response, but causes an impaired raft assembly (Simons et al., 2000; Simons et al., 2002). Excess PLP1 along with other essential parts of myelin are found within lysosomal and endosomal vesicles. Thus, a surplus of PLP1 creates an imbalance in the myelin constituents that negatively affects late stages of myelin formation in the Golgi network (Simons et al., 2002). Myelin in these cells has improper structure due to the incorrect ratios of myelin lipid and protein components, even though they contain normal PLP1.

1.3 Genetics and molecular basis of disease

The disturbance of the myelin formation observed in PMD patients led to the proposal that the disease is attributed to a defect in a myelin protein (Gencic, Abuelo, Ambler, & Hudson, 1989). Scientists began to further investigate mutations of the *PLP1* gene as the cause of PMD after it was mapped to the human X chromosome because of the apparent X linked pattern of inheritance observed in PMD patients (Gencic et al., 1989; Willard & Riordan, 1985). A second piece of strong evidence leading to the investigation of *PLP1* mutations as the cause of PMD, was the discovery that the dysmyelinating mouse mutant *jimpy*, which is pathologically and genetically similar to PMD, has a mutation in the *Plp1* gene resulting in aberrantly spliced *Plp1* transcripts (Morello, Dautigny, Pham-Dinh, & Jolles, 1986; Nave, Bloom, & Milner, 1987). Finally, an immunocytochemistry assay showed an absence of PLP1 in the brain of an 18-year-old patient with PMD (Koeppen, Ronca, Greenfield, & Hans, 1987). Genetic defects in the *PLP1* gene were discovered to be the underlying causative factor of PMD when mutations within this gene were identified in several patients with the disease (Gencic et al., 1989; Trofatter, Dlouhy, DeMyer, Conneally, & Hodes, 1989).

The human *PLP1* gene occupies a 17 kb region of genomic DNA which is located on chromosome Xq22.3 (Koeppen & Robitaille, 2002). The *PLP1* gene consists of seven exons, with exon three containing an internal donor splice site that is used to generate a smaller transcript, *DM20* (Hudson, 2003). The PLP1 protein has

one intracellular and two extracellular loops with four-transmembrane domains, depicted in figure 1.1 (Garbern, 2007; Popot, Pham Dinh, & Dautigny, 1991). There is a 35 amino acid PLP1 specific region that is missing from the intra-cellular loop of DM20, depicted by the blue shading in figure 1.1 (I. R. Griffiths, Montague, & Dickinson, 1995). In the CNS during early embryonic development, DM20 is the major isoform expressed prior to myelination, but it is overtaken by PLP1 postnatally during myelination and into adulthood (Fujimoto, Roots, Burton, & Agrawal, 1976; Timsit et al., 1995). The *PLP1* gene is highly conserved across mammalian species; at the amino acid level there is complete identity between mouse and human PLP1. Therefore, mouse models can be used as faithful representations of this disease, leading to greater understanding of PMD.

Point mutations, insertions, and deletions are known mutations of the *PLP1* gene that cause PMD. However, the most common cause of PMD, accounting for more than 60% of cases, is a large genomic duplication (Sistermans, de Coo, De Wijs, & Van Oost, 1998). These duplications most commonly occur in tandem, and include a large genomic segment that includes the entire *PLP1* gene and neighboring genes (K. Inoue et al., 1996; K. Inoue et al., 1999; K. Woodward, Kendall, Vetrie, & Malcolm, 1998; K. J. Woodward et al., 2005). *PLP1* duplications are presumed to cause disease as a result of an overexpression of PLP1, but this has not yet been confirmed in patients with PMD (Anderson et al., 1998; I. Griffiths et al., 1998; Karim, Barrie, McCulloch, Montague, Edgar, Kirkham, Anderson, Nave, Griffiths, & McLaughlin,

2007). Variations are observed in the size of the duplicated segment among families with the smallest duplication identified at 100 kb and the largest at 5 Mb (K. J. Woodward et al., 2005). Therefore, *PLP1* might not be the only gene that is overexpressed in these patients. In fact, the X-chromosome holds a number of other genes that could also be inappropriately expressed and contribute to the disease phenotype. The minimal set of genes that was found within the smallest duplicated region of a PMD patient was *PLP1*, *GLRA4*, and *TMEM31*. These genes could contribute to the PMD phenotype due to increased gene dosage.

The *PLP1* gene duplication may not only lead to an overexpression, but may also lead to a shift in the *PLP1/(PLP1+DM20)* splicing balance in the direction of the *PLP1* isoform (Regis, Grossi, Corsolini, Biancheri, & Filocamo, 2009). However, the *PLP1/(PLP1+DM20)* expression profile has only been analyzed by Regis et al. and they used fibroblasts from three PMD patients with an extra gene dosage of *PLP1*. Cultured fibroblasts express the *PLP1* gene at very low levels (Regis et al., 2009). Therefore, these results might not be relevant since these findings were obtained using a cell type which only expresses a small amount of *PLP1* transcript and is irrelevant to the disease. This type of analysis should be performed by observing the *PLP1/(PLP1+DM20)* expression profile in tissue of the central nervous system due to the fact that the *PLP1* expression is predominately detected in oligodendrocytes, which are only found in the central nervous system.

1.4 Animal models

Transgenic rodents have been generated in which only the *Plp1* gene is overexpressed, and in these models the severity of the neurological phenotype is proportional to the copy number of the transgene (Anderson et al., 1998; Anderson et al., 1999; Bauer et al., 2002; Bradl et al., 1999; Y. Inoue, Kagawa, Matsumura, Ikenaka, & Mikoshiba, 1996; Karim, Barrie, McCulloch, Montague, Edgar, Kirkham, Anderson, Nave, Griffiths, & McLaughlin, 2007; Karim et al., 2010; Readhead, Schneider, Griffiths, & Nave, 1994). There is no model that resembles a common genomic rearrangement found among PMD patients. A model that faithfully recreates the common tandem genomic duplication that includes *Plp1* will not only provide information about PMD specifically, but also lead to a general understanding of how such duplications would lead to a disease phenotype.

Two mouse models currently exist that contain a tandem duplication, but they model autosomal disease rather than X-linked (Li et al., 2007; Walz, Paylor, Yan, Bi, & Lupski, 2006). These mice have been used to understand how such arrangements lead to a diseased phenotype. A mouse was used to model Down syndrome, and was created using a *Cre/loxP* mediated chromosomal engineering technique to generate a 22.9 Mb duplication (Li et al., 2007). The Down syndrome mouse model had elevated expression of genes within the duplicated region, except for genes that are transcriptionally inactive. Elevated expression of the genes within the duplicated region gives rise to heart and gastrointestinal defects, characteristic of patients with

Down syndrome. The gene or genes that is specifically responsible for the heart and gastrointestinal phenotype has yet to be determined. The second mouse was made using the same chromosomal engineering technique to generate a 3.7 Mb duplication at chromosome 17p11.2 (Walz et al., 2006). Using the model, it was concluded that even though 18 other genes were within the duplicated region, extra gene dosage of *Rai1* was responsible for the physical and behavioral phenotype abnormalities in mice. Our newly characterized mouse model is valuable for the understanding of how genomic rearrangements lead to a disease phenotype, and also will be a valuable model for understanding the skewing of X-inactivation in females since this cannot be tested in existing models.

1.4.1 Existing transgenic models of PMD

The current rodent models that contain extra copies of *Plp1* were made by random integration into the genome of a fragment of a genomic cosmid clone that contained *Plp1*. All of these models carry extra copies of the *Plp1* gene on an autosome, so mice can be either hemizygous or homozygous for the transgene. The different rodent models of PMD are summarized in table 1.1 and are compared to the human duplication which only contains one extra gene copy of *PLP1*.

All of the rodent models carry different numbers of *Plp1* genomic copies, and they showed varying expression levels of *Plp1*. The level of expression does not correlate with the number of genomic copies of *Plp1* in these animals. Since there is

no correlation, this makes it difficult to make predictions about what expression levels might be seen in human patients using these models. For example, the 4e mouse model has two (hemizygous) or four (homozygous) copies of the wild-type *Plp1* gene. In the 4e heterozygous mouse, *Plp1* mRNA levels were expressed at 132% of the wild-type expression levels at postnatal day 19 (P19) (Kagawa et al., 1994). However, the 4e homozygous mouse has 60% *Plp1* mRNA expression compared to wild-type (Kagawa et al., 1994). These results suggest that increased gene dosage of *Plp1* causes an overexpression of mRNA, but a greater increase of gene dosage will begin to decrease expression level. Unfortunately, this hypothesis is rejected when these results are compared to the #66 mouse line that harbors seven (hemizygous) or fourteen (homozygous) copies of the wild-type *Plp1* gene. Based on what was observed in the 4e mouse line, a hypothesis could be made that both the #66 hemizygous and homozygous mice will have lower levels of *Plp1* transcript when compared to wild-type. However, the results showed that the hemizygous mice had 122% and the homozygous mice had 60% *Plp1* mRNA expression compared to wild-type at P20 (Karim, Barrie, McCulloch, Montague, Edgar, Kirkham, Anderson, Nave, Griffiths, & McLaughlin, 2007). In sum, with two and seven copies of *Plp1* there was an overexpression of transcript, and with four and fourteen copies of *Plp1* there was an underexpression of transcript. These results do not show any correlation between gene dosage and RNA levels of *Plp1*. This could be due to the fact that results from the #66

mouse line were obtained from spinal cord tissue, while the 4e mouse line data were obtained from brain.

The #66 mouse line was the only animal model that was used to obtain protein expression levels of PLP1 in the overexpressor animal models. A small increase was observed in PLP1 protein expression in spinal cord from P3 #66 hemizygous mice compared to wild-type (Karim, Barrie, McCulloch, Montague, Edgar, Kirkham, Anderson, Nave, Griffiths, & McLaughlin, 2007). An increase of PLP1 protein was also observed in the #66 homozygous mice compared to wild-type. However, at a later age, P20, the #66 hemizygous mice expressed normal levels of PLP1 protein, while the #66 homozygous mice expressed lower levels compared to wild-type. These results suggest that increased gene dosage of *Plp1* does not alter protein expression levels until a greater increase of gene dosage, which will cause a decrease in protein expression level. Recall in the #66 hemizygous mice, an increase of mRNA levels of *Plp1* were observed and normal protein levels. This suggests there is a translational or post-translation regulation of PLP1 that might occur in these animals. The remaining overexpressor models need to be tested to determine whether there is a correlation between gene dosage and protein expression levels.

The number of *Plp1* copies does appear to correlate with phenotypic severity. Results from experiments with the current rodent models showed that an increase in *Plp1* gene dosage leads to demyelination and hypomyelination phenotypes that worsen with higher dosage number (I. Griffiths et al., 1998). This correlation between gene

dosage and phenotypic severity was also found in humans bearing extra copies of *PLP1*. Patients with three or more copies of the *PLP1* gene have a more severe phenotype than patients with the duplication (Wolf et al., 2005).

Proteins important in the development of myelin have been used as myelination developmental markers to determine if the development of myelin is disrupted due to extra copies of *Plp1*. Expression of other myelin proteins was examined in the #66 mouse line. Increased gene dosage of *Plp1* was shown to decrease the protein expression of MBP, MAG, and CNPase. In the #66 homozygous mice (14 copies of *Plp1*) MBP, CNPase, and MAG all are expressed at 50% or less of the protein expression in wild-type (Karim, Barrie, McCulloch, Montague, Edgar, Kirkham, Anderson, Nave, Griffiths, & McLaughlin, 2007). In the #66 hemizygous mice (7 copies of *Plp1*) MBP expression is 50% of that in wild-type mice, while all the other myelin proteins are expressed at normal levels (Karim, Barrie, McCulloch, Montague, Edgar, Kirkham, Anderson, Nave, Griffiths, & McLaughlin, 2007).

None of these current animal models replicate the human disease; they are all genetically different from PMD patients. Not only does the number of genomic copies of *Plp1* range from two to fourteen, but the adjacent DNA that includes other genes and regulatory elements, is not included. This DNA that is excluded might be important in the regulation of *Plp1* expression.

1.4.2 The *Plp1*dup mouse model of PMD

In this thesis a new model of PMD is characterized. This model is a more faithful representation of the human duplication at the *Plp1* locus that causes PMD compared to previous rodent models. This model contains a 217 kb genomic duplication at the *Plp1* locus and includes the entire *Plp1* gene. This duplication is within the 100 kb to 5 Mb size range and exists in the tandem head to tail arrangement common among PMD patients. Not only does the duplication include only one extra copy of *Plp1* like in the human duplication, but it also includes an extra copy of adjacent DNA including five other genes.

The *Plp1*dup mouse was generated using Mutagenic Insertion and Chromosome Engineering Resource (MICER) technology (Adams et al., 2004) in three steps, summarized in figure 1.2. In the first targeting step, a vector harboring a neomycin (*neo*) selectable marker and the 5' end of the human *hprt* gene separated by a *loxP* site was inserted into a region proximal to *Plp1* by homologous recombination in ES cells from 129/sv/EV mice. ES cells with the insertion were selected by neomycin resistance and used in the second targeting step. The second vector harboring a puromycin (*puro*) selectable marker and the 3' end of the human *hprt* gene separated by a second *loxP* site was targeted to a distal region of *Plp1* by homologous recombination. Puromycin resistant ES cells were used in the third step. *Cre* recombinase was introduced to these cells to cause unequal sister-chromatid exchange at the *loxP* sites on either side of the *Plp1* gene resulting in a tandem duplication (Yu

& Bradley, 2001). This recombination event also brings together the 3' and 5' ends of the *hpert* gene, so cells in which a duplication has occurred have an intact *hpert* gene. ES cells that survived selection by hypoxanthine/aminopterin/thymidine (HAT) resistance were microinjected into C57Bl/6 blastocysts to create chimeras. Chimeras were mated with C57Bl/6J females (The Jackson Laboratory) to determine germline transmission, which could only yield carrier females with the duplication. Carrier females were then bred to male littermates to obtain F2 generation. F2 litters contain four different types of mice, since the duplication is located on the X chromosome, wild-type males, wild-type females, carrier females harboring the duplication on one X chromosome, and males that contain the duplication on their only X chromosome. The males that harbor the duplication, called *Plp1dup*, will be characterized in this thesis as a new mouse model of PMD.

The resulting head to tail tandem duplication was 217 kb in size. This duplication includes the entire *Plp1* gene, as well as five other genes at the *Plp1* locus: *Tceal 3* (transcription elongation factor A, SII-like 3), *Tceal1* (transcription elongation factor A, SII-like 1), BC065397 (transcript within ADP ribosylation factor family), *Morf4l2* (mortality factor 4 like 2), and *Glr4* (glycine receptor, alpha 4 subunit, 2 isoforms). The mouse model was made in the Neurogenetics Research Laboratory at Nemours by Karen Sperle using the services of the Transgenic Core Facility at the University of Delaware and the Transgenic and Gene Targeting Facility at Thomas Jefferson University.

Table 1.1 Summary of phenotype and *Plp1* dosage of existing PMD transgenic rodents and the human disease.

		Human duplication	4e mouse		#72 mouse		#66 mouse		Lew.PLP rat	
		Male	Hemi	Homo	Hemi	Homo	Hemi	Homo	Hemi	Homo
Extra copies of <i>Plp1</i>		1	2	4	3	6	7	14	4-7	8-14
Location of extra		X-Chromosome	autosome	autosome	autosome	autosome	autosome	autosome	autosome	autosome
<i>Plp1</i> RNA levels¹			E16-500% P19-132%	E16-700% P19- 60%		P20, P60- small inc	P20- 122%	P20- 60%		200%
<i>PLP1</i> protein levels¹							P3-small inc. P20-Normal	P3-Increase P20-Small dec.		
Age	Onset	1 yr (9 days ²)	2 months	Birth	1 year	14 days	15 months	Birth	Normal	12 days
	Death	40-60 yr (9 mo- 15 mo ²)	1 year	1 month		5 months		2 months	Normal	
Type of Myelination		Hypomyelination, later demyelination	demyelination	hypomyelination	denyelination	hypomyelination	denyelination	hypomyelination, demyelination		denyelination
Phenotype Reported		Early: poor motor control Later: ataxia, tremor, and spasticity	Late: hindlimb tremors, ataxia, and seizures	Early: hindlimb tremors, ataxia, and seizures	Late: tremor followed by seizures, weakness, and ataxia	Early: tremor followed by seizures, weakness, and ataxia	after 1 year: weight loss, kyphosis, weakness, and ataxia	Second week of life: tremor followed by seizures, weakness, and ataxia	Late: hindlimb tremors, ataxia, and seizures	Early: hindlimb tremors, ataxia, and seizures

Homo = homozygous; Hemi = hemizygous; inc = higher levels; dec = lower levels, blank = not reported

¹Values compared to wt

²Human Age converted to mouse age based on the normal life span of human reported by the CDC, 80 years, and the life span of lab mouse reported by Jackson Laboratory, two years. The assumption was made using these numbers that every mouse year = 40 human years.

References: (Anderson et al., 1998; Anderson et al., 1999; Bradl et al., 1999; Garbern et al., 2002; Garbern, 2007; Kagawa et al., 1994; Karim, Barrie, McCulloch, Montague, Edgar, Kirkham, Anderson, Nave, Griffiths, & McLaughlin, 2007; Koeppen et al., 1987)

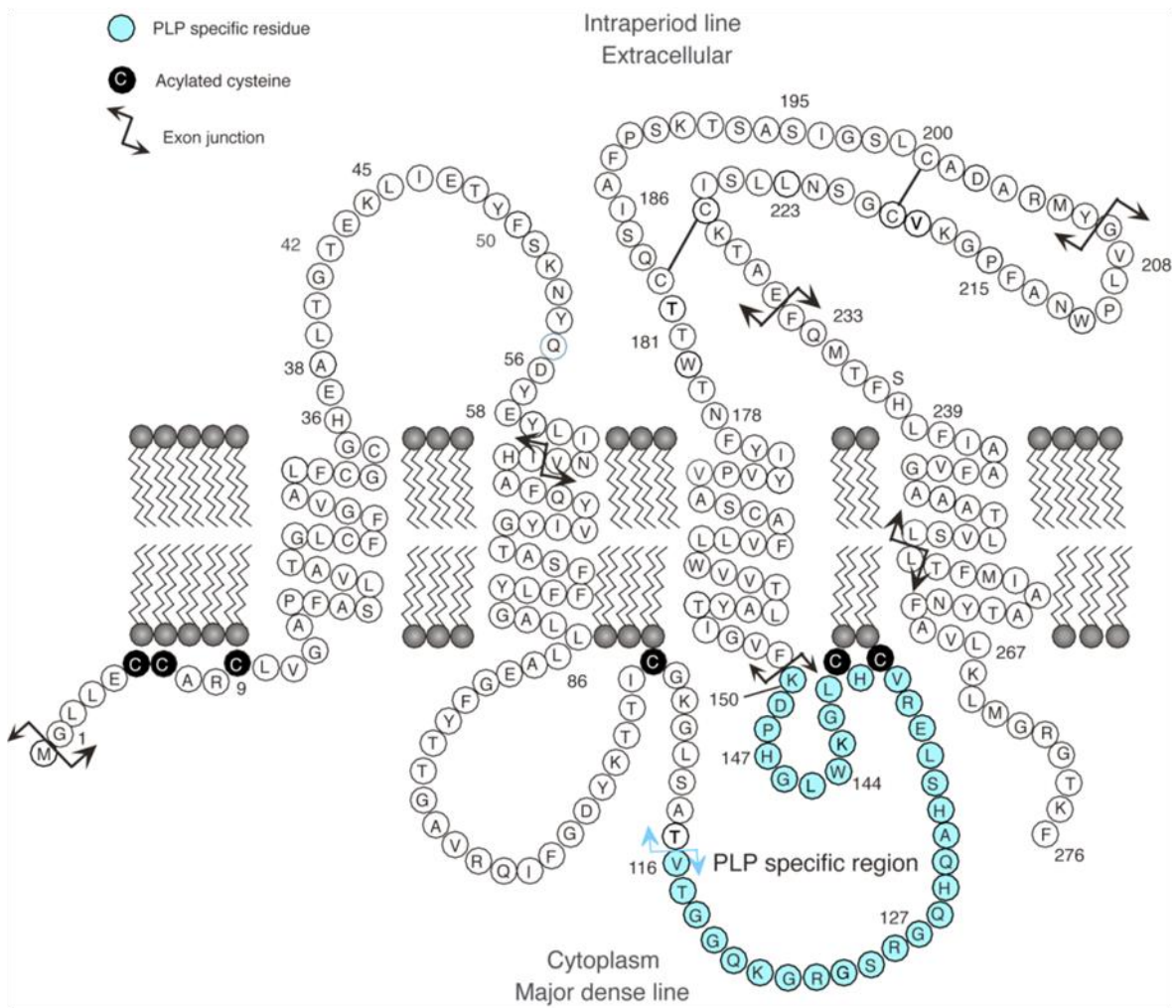


Figure 1.1 Diagram of PLP1. The PLP1 protein consists of four transmembrane domains, two extracellular loops and one cytoplasmic loop. PLP1-specific region shows the region that is missing from the DM20 isoform due to the alternatively spliced RNA and these residues, 117-151, are found within the cytoplasmic loop. Figure used with permission of Dr. James Garbern, University of Rochester Medical Center, Rochester, NY.

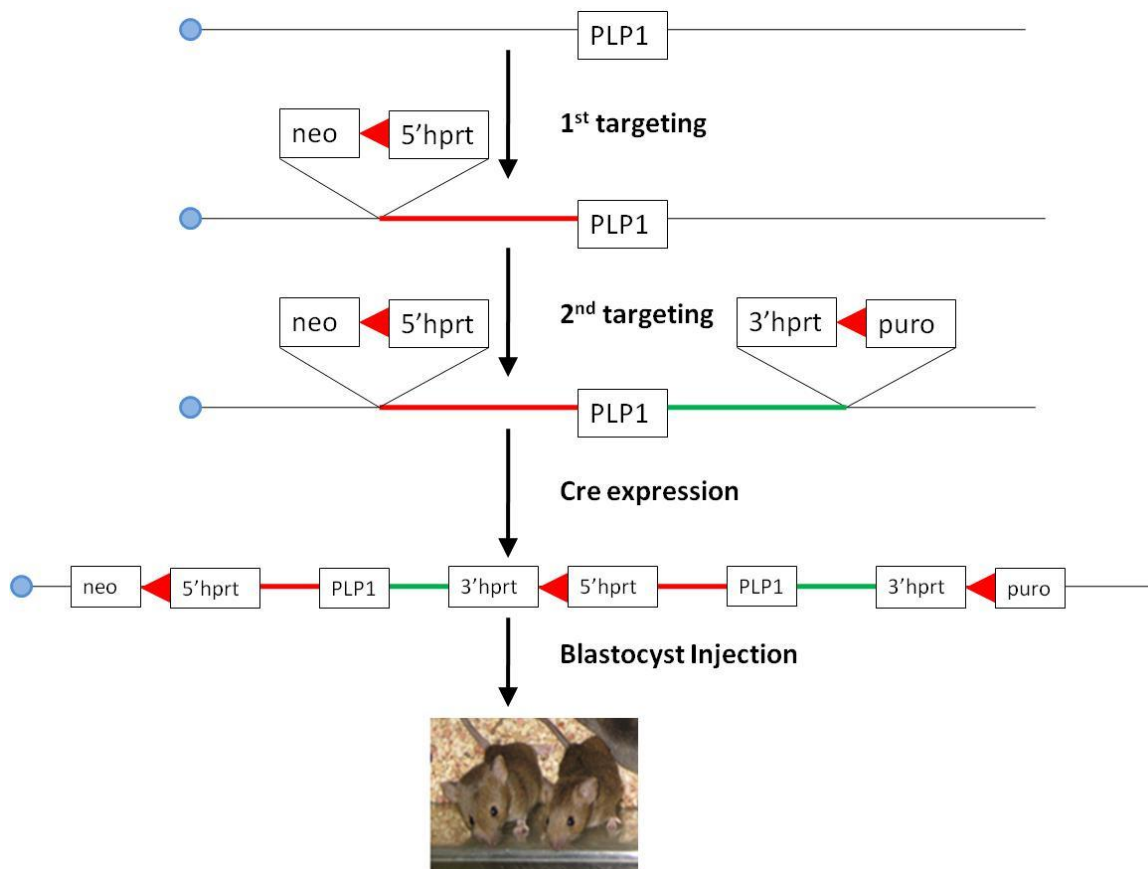


Figure 1.2 Diagram summarizing targeting steps in making of the *Plp1* dup mouse. The *Plp1*dup mouse was generated using Mutagenic Insertion and Chromosome Engineering Resource (MICER) technology (Adams et al., 2004) in three steps. The first targeting step was insertion of a vector harboring an area of homology to a region proximal to *Plp1*, a neomycin (neo) selectable marker, the 5' end of the human *hpert* gene, and a *loxP* site was inserted into ES cells from 129/sv/EV mice. The ES cells were screened for neo resistance and surviving cells were used for the second targeting step. The second targeting step was insertion of a vector harboring an area of homology that allowed it to be inserted distal to *Plp1*, a puromycin (puro) selectable marker, the 3' end of the human *hpert* gene, and a second *loxP* site. The ES cells that survived a screening for puro resistance were used in the third step. The third targeting step was introduction of the *Cre* recombinase into these cells to cause a recombination event at the *loxP* sites on both sides of the *Plp1* gene resulting in a tandem duplication. This recombination also brings together the 3' end of the *hpert* gene to the 5' end, so the cells with the duplication also have an intact *hpert* gene. ES cells that survived selection by hypoxanthine/aminopterin/thymidine (HAT) resistance were microinjected into C57Bl/6 blastocysts to create chimeras. Blue circle: position of centromere, thick red line: duplicated portion proximal of *Plp1*, thick green line: duplicated portion distal of *Plp1*, red triangle: *loxP* site, neo^R: neo resistance, puro^R: puro resistance, HAT^R: HAT resistance.

Chapter 2

MATERIALS AND METHODS

2.1 Mice

The mouse colony was maintained in the Life Science Center at Alfred I. duPont Hospital/Nemours, and kept to a diet of water and standard mouse chow ad libitum. The B6.129 – Dp(XTceal3-Plp1)1Tju mouse strain or *Plp1*dup was generated using 129/Sv/Ev ES cells that were engineered to harbor a duplication at the *Plp1* locus (for details refer to section 1.4.2 in the introduction) and microinjected into C57Bl/6 blastocysts to make the chimeras. Chimeras were mated with C57Bl/6 mice to produce the F1 generation. Identification of germline transmission was done by selecting pups from the F1 generation with the agouti coat color, and the selected females were mated with male littermates with black coat color to produce the mixed background F2 generation. Carrier F2 females were mated with mixed background wild-type males, either males from the F1 generation or B6129SF1/J (The Jackson Laboratory), to maintain the line on a mixed background.

2.2 Genotyping

2.2.1 Nucleic acid isolation and purification

Genotyping was done using two methods, densitometry and capillary electrophoresis, on DNA obtained from tail-snips and spleen. Results obtained using the first two methods were then confirmed by identifying the formation of a complete human *hprt* gene generated during the formation of the duplication.

DNA was isolated from tail snips collected at weaning using DNeasy Blood and Tissue Kit (Qiagen, Valencia, CA) following the manufacturer's protocol for genotyping the mice. DNA was isolated from spleen tissue using Genra Puregene Tissue Kit (Qiagen) following the manufacturer's protocol when mice were euthanized for RNA and protein expression experiments. Nucleic acid concentrations were measured using Nanodrop spectrophotometer (Thermo Scientific, Hampton, NH), and a 260/280 ratio of approximately 1.80 was verified.

2.2.2 Genotyping analysis

Semi-quantitative multiplex PCR was performed on DNA from spleen and tail snips by completing 25 cycles of PCR using a Multiplex PCR Kit (Qiagen) according to manufacturer's instructions. All primer pairs used for genotyping are listed in Table 2.1. Gender was determined by amplifying a region of the Y-chromosome using the mSRY-F and mSRY-R primer pair. A region of *Plp1* gene was amplified using the

mPLP-F6 and mPLP-R1 primer pair, and a region on the proximal end of the generated duplication (region x on figure 3.1.a) was amplified using 197O15-F and 197O15-R primer pair. The amplification of a region of *Plp1* and region x were compared to the amplification of a region of the dystrophin gene (mDMD-28F and mDMD-28R primer pair), which is located a distance from *Plp1*, and was used as an internal single copy control. Regions of the *neo* and *puro* genes were amplified using the neo-F and neo-R primer pair and the MHPP-F14 MHPP-R5 primer pair, respectively. Since *neo* and *puro* were inserted into the genome during the engineering of the duplication, only the mice that have the duplication contain a copy of these genes. This was used as a secondary verification of the duplication genotype.

The multiplex PCR products produced from the amplification using the six primer pairs on the DNA isolated from tail snips were separated using 4% agarose gel electrophoresis. The gel was stained with ethidium bromide and net intensity of the products was obtained using the Gel Doc XR system and software (BioRad, Hercules, CA). Copy number was determined to distinguish *Plp1*dup mice from wild-type mice by analyzing the net intensity or area under the peak data obtained. The test region was first divided by the dystrophin single copy control region. Then this ratio was normalized by dividing it by the average ratio calculated of two wild-type control mice. If the two test regions are duplicated, the expected normalized ratio of the region to the dystrophin control is 2, and if it is not duplicated, then the expected ratio is 1.

The multiplex PCR products produced from the amplification using the six primer pairs on the DNA isolated from spleen were first separated by 4% agarose gel electrophoresis to verify that the amplification was successful before obtaining quantitative data using capillary electrophoresis. Products were detected and analyzed by capillary electrophoresis using the 3130x1 Genetic Analyzer (Applied Biosystems, Carlsbad, CA). This detection was possible due to the reverse primer in each pair being FAM labeled, and area under the peak was obtained using Peak Scanner Software (Applied Biosystems) for analysis. Copy number was determined as above except that the area under the peak was used rather than net intensity.

As further confirmation of the genotype, it was determined that the human *hprt* gene was present in the mice using the DNA isolated from spleen. Using the Expand High Fidelity PCR system (Roche, Basel, Switzerland) and a touchdown PCR technique, amplification of an intact *hprt* gene (hHPRT-F2 and hHPRT-R primer pair) can only occur in DNA from mice harboring the duplication, due to Cre-mediated recombination step that produced the intact human *hprt* gene (figure 1.2).

2.3 RNA expression

2.3.1 Nucleic acid isolation and purification

For RNA expression experiments, half brain cut along the sagittal plane was obtained from postnatal day 1, 7, 10, 12, 14, 21, 60 and 120 (P1, P7, P10, P12, P14, P21, P60 and P120) male mice. This age set allowed for visualization of a developmental time course when myelin rapidly accumulates from postnatal day 10-30 and reaches a higher synthesis rate at approximately day 21 to 23 and into adulthood (Costantino-Ceccarini & Morell, 1972). For these expression experiments, biological replicates of three wild-type and three *Plp1dup* mice were used. Brain tissue was isolated, snap frozen, and stored at -80 °C.

RNA was isolated using RNeasy Midi Kit (Qiagen) following the manufacturer's protocol. RNA was then DNase treated using TURBO DNA-*free* kit (Ambion, Austin, TX) following the manufacturer's protocol. A Nanodrop spectrophotometer (Thermo Scientific) was used to determine nucleic acid concentration, and to ensure that 260/280 ratios were approximately 2.00. The total RNA quality was obtained by RIN algorithm (RNA Integrity Number) using the 2100 Bioanalyzer and the RNA 6000 Nano Chip kit (Agilent, Santa Clara, CA), following manufacturer's protocol. If a RIN number of seven or above was obtained, then the quality of the RNA was sufficient for qRT-PCR.

2.3.2 Semi-quantitative and real-time quantitative RT-PCR

One microgram of total RNA was denatured of secondary structure at 65 °C for 5 minutes. The total RNA was then reverse transcribed in a 20 µl reaction at 37 °C for 60 minutes using the Omniscript reverse transcription kit (Qiagen) following the manufacturer's protocols. All cDNA was stored at -20°C and used for both semi-quantitative and real-time quantitative RT-PCR experiments.

Semi-quantitative multiplex PCR was performed with 1 µg of cDNA prepared from mouse brain RNA using the Multiplex PCR Kit (Qiagen). The RT-PCR was carried out using the following protocol: 15 minutes at 95 °C, followed by 24 cycles (P1 using 30 cycles) of 45 seconds at 94 °C, 1.5 minutes at 60 °C, and 1.5 minutes at 72 °C, then ending with 10 minutes at 72 °C. PCR products were stored indefinitely at 4 °C. The primer pair mPLP2-F1 and mPLP4-R2 was used to amplify both *Plp1* and *Dm20* transcripts, as this primer pair yields different sized products from these splice variants. To ensure that equal amounts of RNA were used, the endogenous control β -actin was amplified with the mACTb-F2 and mACTb-R primer pair. Products were detected and analyzed by capillary electrophoresis using the 3130x1 Genetic Analyzer (Applied Biosystems). This detection was possible due to the reverse primer in each pair being FAM labeled, and Peak Scanner Software (Applied Biosystems) was used for the analyses. The splice ratio was determined by analyzing the peak areas using the following equation: $(Plp1/(Plp1+Dm20))$.

Real-time quantitative RT-PCR was performed for quantification of mRNA expression of *Plp1*, mRNA expression from the five other genes within the duplication, and the mRNA expression of myelin proteins *Mag*, *Mbp*, and *CNPase* using QuantiTect SYBR Green PCR kit (Qiagen) following the manufacturer's instructions. In each experiment, 0.5 µg cDNA was used for each reaction, performed in 20 µl triplicates for each sample, using three biological replicates of wild-type and *Plp1dup* mice at each age. The following QuantiTect Primer Assays (Qiagen) were used according to the manufacturer's instructions: Mm_Plp1_1_SG, Mm_Glra4_1_SG, Mm_Tceal1_3_SG, Mm_Tceal3_1_SG, Mm_Morf4l2_1_SG, Mm_BC065397_2_SG, Mm_Mbp_1_SG, Mm_Mag_1_SG, and Mm_Cnp_1_SG. The primer assays mus musculus calnexin (CANX) and mus musculus cytochrome c-1 (CYC1) were used to amplify endogenous controls (PrimerDesign, Southampton, UK) (see appendix for selection process). qRT-PCR was carried out using the ABI prism 9700 (Applied Biosystems, Foster City, CA) with an initial denaturation step at 95 °C for 15 min to insure complete activation of the hot start DNA polymerase, followed by 40 cycles of 94°C for 1 min, 55°C for 30 seconds, and 72°C for 30 seconds. The specificity of amplified product was confirmed by a melting curve analysis, which included an initial denaturation step at 95°C for 15 seconds, an annealing step at 60°C for 15 seconds, and finally a gradual increase to 95°C (2% ramp rate) to denature again.

Calculations of qRT-PCR were performed by first obtaining Ct values detected during amplification using 9700 SDS RQ software (Applied Biosystems) for each transcript. All transcripts of interest were normalized by dividing raw Ct values for each sample by the appropriate normalization factor calculated from the geometric mean of the two most stable house-keeping genes CANX and CYC1. As shown in the Appendix, the most stable house-keeping genes were selected using geNorm application for Excel (Microsoft) which is available for public use at <http://medgen.ugent.be/~jvdesomp/genorm/>. Relative quantification (RQ) of RNA expression in the *Plp1*dup mouse was determined using the average of the three wild-type males as the calibrator DataAssist Software v2.0 (Applied Biosystems) with the $2^{-\Delta\Delta CT}$ method. The relative amounts of mRNA for each transcript were expressed as a percentage of wild-type using the average RQ values for *Plp1*dup mice at each time point. A program was developed using the Statistical Analysis System SAS (SAS Institute Inc, Cary, North Carolina) to analyze the raw Ct values. Statistical significance between wild-type and *Plp1*dup mice RNA expression levels was determined using a standard ANOVA test. Standard deviations were calculated and used to show variation between mice.

To determine the developmental expression pattern of *Plp1* in the brain, the same qRT-PCR procedure was used. However, only CYC1 was used as the endogenous control due to space constraints on a single plate. Relative quantification (RQ) of the RNA levels at each time point was determined using the average of the 3

wild-type P1 males as the calibrator using DataAssist Software (Applied Biosystems) v2.0 with the $2^{-\Delta\Delta CT}$ method. The relative amounts of *Plp1* mRNA were expressed as a fold change relative to P1 wild-type expression using the average RQ values for each time point. This allowed for a visualization of the expression of *Plp1* after P1 in wild-type and *Plp1dup* mice. Standard deviations were calculated as described above.

2.4 Protein expression

2.4.1 Protein isolation

For protein expression experiments, half brain cut along the sagittal plane was obtained from P1, P7, P10, P12, P14, P21, P60 and P120 male mice, as described for the RNA expression analysis. Biological replicates of three wild-type and *Plp1dup* mice were also used. Brain tissue was isolated, snap frozen, and stored at -80 °C.

Protein extracts were prepared from mouse brain by homogenization in suspension buffer which contained 0.1M NaCl, 0.01M Tris-Cl (pH7.6), 0.001M EDTA(pH 8.0) and addition of 100µl of protease inhibitor (Thermo Scientific) per 10mL of buffer at time of use. An equal amount of 2x SDS Gel Loading Buffer which contained 100mM Tris-Cl (pH 6.8), 4% SDS, 20% glycerol, and 200mM DTT was added to the homogenate and mixed well by inversion and vortexing. The homogenate was sonicated ten pulses of 1 sec each, and then centrifuged at 5,000 x g for 5 minutes and supernatant liquid was removed and used as the protein lysate. Protein

concentration was determined by measuring absorbance at 280 using a Nanodrop spectrophotometer (Thermo Scientific).

2.4.2 Western analysis

30 µg of protein was separated on 4-20% GTX gel (BioRad) and transferred to a PVDF membrane (Invitrogen, Carlsbad, California). Membranes were probed with mouse monoclonal antibodies anti-PLP1 at a dilution of 1:2000 (AA3 Hybridoma, a kind gift from Dr. Alexander Gow, Wayne State University), anti-MBP at 1:1000 (Millipore, Cat#09-849), anti-CNPase at 1:5000 (Covance, SMI-91R), anti-MAG at 1:1000 (Millipore, Cat#MAB1567), and anti-GAPDH at 1:20000 (Sigma, Cat#G8795). Membranes were then incubated in DyLight-405 (Jackson ImmunoResearch), Cy3-, or Cy5-labeled (GE Healthcare, Piscataway, NJ) secondary antibody diluted 1:2500. Fluorescently labeled protein was detected using the Typhoon Trio scanner (GE Healthcare). When DyLight-405 or Cy5 secondary was used, the 633nm wavelength laser was selected to visualize the protein, but when Cy3 secondary was used, the 532nm wavelength laser was selected. Bands were quantified using ImageQuant TL v2003.03 software (GE Healthcare) with GAPDH as a control for loading accuracy. Relative amounts of protein from *Plp1*dup mice were expressed as a percentage of wild-type.

2.5 Pathology

For pathology experiments all mice were anesthetized then perfused with fixative before brain tissue was harvest. The mice that were used in these experiments were one, three, and six months of age, and tail-snip DNA was used to identify mice needed for experiments. Biological replicates of 2-4 wild-type and *Plp1*dup mice were used for observation in these experiments.

2.5.1 Histology

Animals were anesthetized with 4 μ l of 50mg/ μ l ketamine, 20mg/ μ l xylazine per gram of body weight by intraperitoneal (IP) injection. Each animal was completely perfused through the left ventricle with 2.5ml of 4% paraformaldehyde in 0.1M PBS per gram of body weight slowly using a pump. The brain was then isolated and placed in 4% paraformaldehyde in 0.1M PBS buffer at 4 °C. The brain was sliced with a razor blade in 2 mm coronal sections and submitted to the Histotechnology Core at A. I. duPont Hospital/Nemours Children's Clinic for processing, sectioning, and staining. The sample was taken through a series of graded alcohols, cleared and infiltrated with paraffin on the Leica ASP300 tissue processor (Leica Microsystems Inc, Buffalo Grove, IL). Tissues were embedded in paraffin on the Leica EG1160 embedder (Leica Microsystems Inc). Samples were cut in 5 μ m sections on the Leciva

RM2255 microtome (Leica Microsystems Inc). Sections were stained with Luxol Fast Blue-Periodic Acid Schiff's-Hematoxylin (LFB/PAS) procedure (Sheehan and Hrapchak, 1980), which was used to visualize the myelin content.

2.5.2 Confocal and electron microscopy (EM)

Brain and spinal cord tissues were used to visualize myelin formation by confocal and electron microscopy to obtain a detailed view of myelination in the *Plp1dup* mice compared to wild-type mice. Animals were anesthetized, as described in 2.5.1. Each animal was completely perfused through the left ventricle with 2.5ml of 4% paraformaldehyde and 0.5% glutaraldehyde in 0.1M PBS per gram of body weight slowly using a pump. After perfusion, brain and spinal cord were removed and placed in fixative for at least 24 hours.

Spinal cord was sent to Dr. Robert Skoff (Wayne State University) for EM processing and analysis. The spinal cords were dissected transversely into 1mm pieces and processed as follows. Tissues were rinsed in 0.1M phosphate buffer 3 x 10 min, fixed with 1% osmium tetroxide (Electron Microscopy Sciences, Hatfield, PA) for 2 hrs. They were rinsed again with 0.1M phosphate buffer 3 x 10 min and dehydrated with increasing percentages of ethanol for 2 x 5 min up to 100% for 3 x 10 min and then with propylene oxide (Electron Microscopy Sciences) 3 x 10min.

Tissues were then infiltrated overnight with a 1:1 solution of propylene oxide and Araldite 502 (Electron Microscopy Sciences), then embedded the next day with 100% Araldite and cured at 60 °C for 48 hrs. Ultra-thin sections were cut on an Ultracut E microtome (Reichert Technologies, Depew, NY) using a glass knife and diamond knife respectively. These ultra-thin sections were stained with uranyl acetate (Electron Microscopy Sciences) and lead citrate (Polysciences, Warrington, PA) and visualized and imaged using Jeol 1010 electron microscope to visualize.

Brain tissues were infiltrated with 2.3M sucrose in 0.1 M Sorensen's phosphate buffer. Samples were then embedded in cryomolds with Tissue Freezing Medium (Electron Microscopy Sciences), frozen at -30 °C, and stored at -80°C until sectioned. A CryoStat (Leica Microsystems, Wetzlar, Germany) was used to prepare sections 20um thick using the CryoJane Tape-Transfer system (Leica Microsystems). Sections were stained using a BrainStain Imaging Kit (Invitrogen), which contained FluoroMyelin green fluorescent myelin stain, NeuroTrace 530/615 red fluorescent Nissl stain, and DMSO DAPI dihydrochloride, following the manufacturer's protocol.

2.6 X-Ray analysis

Mice were anesthetized with 3-5% isoflurane and placed in the In-Vivo Imaging Systems (Carestream, Rochester, NY) cabinet. They were maintained with 2% isoflurane through-out the analysis period. X-ray images were obtained using the KODAK 1D Imaging System software (Carestream Health, Inc.). Afterwards, the mice were removed from the isoflurane and monitored until completely recovered.

Table 2.1. Primers used for genotyping and RT-PCR.

Genotyping	
Primer Name	Sequence
mSRY-F	5'-GCATTTATGGTGTGGTCCCGTG-3'
mSRY-R	5'-GCTCTACTCCAGTCTTGCCTGTATG-3'
mPLP-F6	5'-CCACCTGTTTATTGCTGCGTTTG-3'
mPLP-R1	5'-GCACACTGCATTGGCACTACATTAAC-3'
197O15-F	5'-AATGTCTGGGTAGGGTGCTTGTC-3'
197O15-R	5'-AAGAACGGAGATGCTGTTAGATGAG-3'
mDMD-28F	5'-GCAGACAGAAAATCCCAAAGAGC-3'
mDMD-28R	5'-TTGTGCTAACTTCATTCCACCAAG-3'
neo-F	5'-GATGATCTGGACGAAGAGCATCAG-3'
neo-R	5'-TAAAGCACGAGGAAGCGGTCAG-3'
MHPP-F14	5'-GCCTTCCATCTGTTGCTGCG-3'
MHPP-R5	5'-GCTGCAAGAACTCTCCTCACG-3'
hHPRT-F2	5'-GCTGAGGATTTGGAAAGGGTG-3'
hHPRT-R	5'-CCTTGAGCACACAGAGGGCTAC-3'
RT-PCR	
Primer Name	Sequence
mPLP2-F1	5'-CTACTGGATGTGCCTGACTGTTTCC-3'
mPLP4-R2	5'-GGGAAGAAACCTCTCTGGTTTCAG-3'
mACTb-F2/R	5'-GTGACGTTGACATCCGTAAAGACC-3'
mACTb-R	5'-AAGAAAGGGTGTAACGCAGCTC-3'

Chapter 3

RESULTS

3.1 Validation of duplication

Figure 3.1 and table 3.1 show the results of two methods that were used to confirm the duplication in *Plp1*dup mice. In one method, semi-quantitative multiplex PCR was performed on the spleen DNA to determine gender using a primer pair that amplifies a region of the Y-chromosome. To determine genotype, a region of the *Plp1* gene as well as a region on the proximal end of the generated duplication (region x) were amplified for comparison to the amplification of a region of the dystrophin gene. In addition, regions of the *neo* and *puro* genes were amplified to verify the duplication since they were inserted into the genome during the engineering of the duplication. Figure 3.1a depicts where the primer pairs anneal. PCR products were separated by gel electrophoresis and stained with ethidium bromide for visualization before submitting the samples for capillary electrophoresis (figure 3.1b). Males containing the duplication were easily identified in figure 3.1b based on the amplification of *neo* and *puro* (samples in lanes 2, 4 and 5). Results showed that the mice had a greater amplification of the *Plp1* gene and region x compared to the amplification of the dystrophin gene as observed by visualization of the bands. Quantitative data for these

PCR products was obtained by capillary electrophoresis and analyzed by measuring the area under the peak (table 3.1). The values obtained for the *Plp1* region and region x were divided by the value obtained for dystrophin and then the ratio was normalized to the ratio of two wild-type control mice. If the test regions are duplicated, the expected normalized ratio to the dystrophin control is 2. If it is not duplicated, then the expected ratio is 1. Table 3.1 shows this analysis and these data indicate that pups 2, 4, and 5 must harbor the duplication. The genotyping that was performed using DNA isolated from tail snips was similar with the exception that quantitation was performed using densitometry of the ethidium bromide-stained gels instead of by capillary electrophoresis.

For a second analysis done by gel electrophoresis, the presence of the duplication was confirmed by amplification of *hpert* gene using the primers, hHPRT-F2 and hHPRT-R. The *hpert* gene was generated during the recombination event that produced the duplication, as depicted in figure 3.1a. Figure 3.1c shows representative data of the amplified *hpert* product on an agarose gel. Once this product was confirmed, the mouse was identified as a *Plp1dup* mouse.

3.2 *Plp1dup* mice have a distinct physical phenotype due to a chromosomal duplication in the *Plp1* locus that includes the entire *Plp1* gene

At early ages, *Plp1dup* mice do not have a overtly abnormal phenotype, but slight differences were noticed during handling and weaning of three week old mice. For example, while a wild-type male was being held by the tail, he would lift himself

up to clasp the holder's hand. However, the *Plp1dup* males have a more difficult time with this task, and some cannot even lift themselves up completely.

At six months of age, obvious weight differences were observed in *Plp1dup* males compared to wild-type littermates. Figure 3.2 shows that *Plp1dup* males at six months of age have a lower body weight compared to wild-type littermates. *Plp1dup* males weigh an average 35.25 g while wild-type males were slightly heavier averaging 41.22g. There was a statistically significant difference observed in the weights of the two groups of mice.

At five months of age and older, a slight curvature of the spine was observed as a hump in *Plp1dup* males that was not present in wild-type males. An X-ray analysis was performed on three five month old male mice, one wild-type and two *Plp1dup*, and the results are presented in figure 3.3. As shown by the red arrow, the hump was seen by X-ray analysis. However, in these data, two *Plp1dup* males were analyzed, and only one has this altered curvature in the spine. It was not clear if the other *Plp1dup* male will develop this phenotype at a later age, or if the hump will never develop.

When *Plp1dup* males were over one year old, they develop seizures more often than wild-type littermates and usually die at this time. This appeared in five of seven *Plp1dup* mice that were kept to a year old. Only two out of seven wild-type littermates developed seizures. Therefore, this appears to be a phenotype that is more

common in *Plp1*dup males compared to wild-type. The lab is currently working on quantifying and statistically analyzing this phenotype in a greater sample size.

3.3 A chromosomal duplication in the *Plp1* locus that includes the entire *Plp1* gene alters expression of PLP1

3.3.1 The duplication alters *Plp1* mRNA expression

The developmental expression of *Plp1* in the mouse brain was investigated to determine the normal expression pattern of *Plp1* during the formation of myelin and into adulthood to elucidate the effect of a duplication on *Plp1* expression. Real-time quantitative PCR (qRT-PCR) was performed to observe the developmental expression of *Plp1*. The results of the analysis of *Plp1+Dm20* at each time point relative to P1 wild-type expression is presented in figure 3.4. A triphasic pattern was observed in the wild-type mice. The initial phase consisted of a period of regular increase in the level of *Plp1+Dm20* mRNA from P1 to P12. During the second phase, a more dramatic increase in total *Plp1+Dm20* transcript was observed from P12 to P21. This was followed by a sharp decline in the level of *Plp1+Dm20* mRNA reaching a constant level at P60. The peak of *Plp1+Dm20* mRNA expression occurred at P21 in wild-type mice. However, a very different expression profile was observed in the *Plp1*dup mouse. An initial phase of a regular increase in the level of mRNA was observed from P1 to P10 that does not appear very different from the wt. However, at P12 to P14, a more dramatic increase in expression of *Plp1+Dm20* mRNA was observed in the *Plp1*dup mice than the wild-type mice. At P21, the *Plp1*dup mouse mRNA was expressed at the same level as the wt. Finally, a slight decline, not as sharp as in the

wt, was observed at P60. Expression does not level out as in wild-type, but shows a dramatic increase in mRNA levels again into P120. These results show very different developmental expression profile of *Plp1+Dm20* mRNA in wild-type and the *Plp1dup* mice.

qRT-PCR was performed on the developmental set of brain RNAs to demonstrate whether the total amount of *Plp1+Dm20* message in the *Plp1dup* mouse was elevated at specific developmental time points compared to wild-type. Quantitative data in figure 3.5a shows that *Plp1+Dm20* mRNA levels were elevated in *Plp1dup* to approximately 200% of wild-type expression levels. This increase was observed at P12, P14, P60, and P120. At the earlier developmental time points, P1, P7, and P10, *Plp1+Dm20* message levels in *Plp1dup* mice were not significantly different from wild-type. At P21, where the *Plp1+Dm20* transcript peaks in wild-type (figure 3.4), the *Plp1dup* mouse shows similar levels of the *Plp1+Dm20* message to the wild-type mice.

3.3.2 The duplication alters PLP1 and DM20 protein expression at P12

Protein expression levels of *PLP1* in the *Plp1dup* brain were examined by Western blot analysis using brain homogenates with a monoclonal antibody (AA3) that recognizes both PLP1 and DM20 isoforms. A monoclonal antibody that recognizes GAPDH was used to verify loading accuracy. Results of the analysis are shown in figure 3.5b. Protein levels were too low to detect until P12 in the

developmental set in *Plp1*dup and wild-type mice. Total PLP1+DM20 protein levels were elevated at P12 in the *Plp1*dup mice, while levels were the same as wild-type mice at P14, P21, P60, and P120. The duplication alters the PLP1 protein expression at P12 only. This suggests that *Plp1* gene expression is a controlled and regulated process.

3.3.3 The duplication does not alter the *Plp1*/(*Plp1*+*Dm20*) splice ratio

To determine whether the duplication in the *Plp1* locus impairs the *Plp1*/*Dm20* splicing ratio, the *Plp1* and *Dm20* transcripts were examined by RT-PCR in RNA prepared from brain of *Plp1*dup and wild-type postnatal brain. The expression level of just the *Plp1* isoform divided by total *Plp1* (*Plp1*+*Dm20*) was calculated and similar expression levels of the *Plp1* isoform were observed in the *Plp1*dup mouse compared to wild-type (figure 3.6). At P1, *Plp1* isoform was approximately 30% of the total *Plp1*/*Dm20* transcript expressed in wild-type and *Plp1*dup mice. At P7 and older, the *Plp1* isoform was approximately 70% of the total *Plp1*/*Dm20* message transcribed in the wild-type and *Plp1*dup mice. The duplication does not alter the splice ratio of the *Plp1* transcripts.

3.4 A duplication in the *Plp1* locus that includes the entire *Plp1* gene alters expression of four of the five other genes found within the duplication

The most common cause of PMD is duplication of a region of the X chromosome that includes the entire *Plp1* gene and the duplicated regions vary in size

and gene content; therefore, it was important to determine if the duplication affects the expression level of other genes within the duplication. The five other genes within the *Plp1*dup mouse duplication were measured at a transcriptional level using qRT-PCR. Transcription elongation factor A (SII-like) 3 (*Tceal3*), transcription elongation factor A (SII-like) 1 (*Tceal1*), mortality factor 4-like 2 (*Morf4l2*), *BC065397*, and glycine receptor subunit alpha 4 (*Glra4*) message levels were obtained using RNA isolated from brains of the developmental set of *Plp1*dup and wild-type mice by qRT-PCR. Figure 3.7a shows the duplication in the *Plp1*dup mice to help visualize the location of each gene relative the *Plp1* gene.

Elevated transcript levels of *Tceal3*, *Tceal1*, *Morf4l2*, and *BC065397* were observed in the *Plp1*dup mice compared to wild-type mice at all postnatal time points except P1 (figure 3.7b, c, d, and e). Expression of *Tceal3* was observed to be 200-250% of wild-type in the *Plp1*dup mouse at most of the developmental set (figure 3.7b). Some variation among the biological replicates lead to no significance difference in *Tceal3* mRNA expression at P10 in *Plp1*dup mouse compared to wild-type. Levels of 200% that of wild-type mRNA was observed among the developmental set of *Tceal1* and *BC065397* in *Plp1*dup mice (figure 3.7c and e). Levels that were 200% of wild-type was observed for *Morf4l2* mRNA. However, variation among replicates lead to no significant difference in *Morf4l2* mRNA levels in *Plp1*dup mouse compared to wild-type at P7. Interestingly, at P120 *Morf4l2* mRNA levels were elevated to 350% of wild-type expression in *Plp1*dup mice. Unlike the

other genes within the duplication, a change in the *Gra4* message levels was not observed in the *Plp1*dup mouse (figure 3.7f). A duplication in the *Plp1* locus alters the expression of four of the five genes found within the duplication not including *Plp1*.

3.5 A duplication in the *Plp1* locus that includes the entire *Plp1* gene affects expression of other myelin proteins

To determine whether changes in *Plp1* gene dosage due to a chromosomal duplication affects the expression of other representative myelin proteins, CNPase, MAG, and MBP transcript and protein levels were measured in the *Plp1*dup mice at the developmental time set and compared to those of wild-type. qRT-PCR was performed with the developmental set of RNA from brain and Western blot analysis with brain homogenates from *Plp1*dup mice and compared to wild-type mice.

The data from real time qRT-PCR shows that the *Plp1*dup mice have expression of CNPase message that was similar to that of the wild-type mice (Figure 3.8a). The only significant difference between *Plp1*dup mice compared to wild-type mice was observed at P21, where transcript levels were decreased. Figure 3.8b shows CNPase protein expression over the developmental time course. It was expressed at P7 and later. *Plp1*dup mice express statistically significant lower levels of CNPase at P60 and P120 compared to wild-type mice.

The data from real time qRT-PCR shows that *Plp1*dup mice have similar MAG expression compared to wild-type mice throughout the developmental time course

(Figure 3.9a). MAG protein expression was found to be altered along the developmental set (figure 3.9b). *Plp1dup* mice express significantly lower levels of MAG at P7, P10, and P21.

The real time qRT-PCR shows that *Plp1dup* mice show a slight decrease in expression of MBP mRNA compared to wild-type mice (Figure 3.10a). P7, P21, and P60 showed significantly lower *Mbp* mRNA levels in *Plp1dup* mice compared to wild-type. MBP protein expression was not observed until P21 (figure 3.10b). *Plp1dup* mice express lower levels of MBP at all the time points compared to wild-type mice, and levels of expression were significantly lower at P60 and P120. A duplication in the *Plp1* locus alters the expression of MBP, MAG, and CNPase.

3.6. A duplication in the *Plp1* locus that includes the entire *Plp1* gene disrupts normal myelin formation

Standard histological analysis was performed to assess the extent and onset of myelin in the *Plp1dup* mice. Whole brains from three wild-type and three *Plp1dup* males at one, three, and six months were coronally sectioned and stained with Luxol fast blue and Periodic acid shift (LFB/PAS) to provide an estimation of myelin content. The LFB stain helped visualize by staining myelin blue and PAS was used as a pink counter stain.

Disruption of normal myelin formation was observed in the corpus callosum of the *Plp1dup* mice. Figure 3.11 shows this histological analysis, and an even myelin pattern was observed in the sections from the wild-type mice. However, a disrupted

discontinuous pattern was seen in the sections from the *Plp1dup* mice. This discontinuous pattern was observed as early as one month (figure 3.11a). At three months, this discontinuous pattern was much more dramatic in the *Plp1dup* sections (figure 3.11b). Sections from wild-type mice at three months show the corpus callosum with a solid even myelin pattern as shown by the blue stain, while the *Plp1dup* mouse has gaps in the blue stain throughout the corpus callosum. Finally, six month old mouse brain sections were observed, and again the same dramatic discontinuous pattern was observed in the *Plp1dup* brains. Figure 3.11c shows the solid and even myelin pattern in the six month wild-type mice, while the six month *Plp1dup* mice show areas of non-myelination within the corpus callosum. Interestingly, *Plp1dup* six month mouse sections also showed round holes within the tissue in myelinated areas (figure 3.11c). The holes were seen along the myelin pattern in the corpus callosum. This could be artifact from the histology processing, but if it was then it was probably due to a difference in the *Plp1dup* mice compared to the wild-type mice at this age because it was only seen in the *Plp1dup* mice.

Although not as obvious as in the corpus callosum, a disruption in normal myelin formation was also observed in the white matter tracks in the cerebellum. Figure 3.12 shows the white matter tracks in the cerebellum of wild-type and *Plp1dup* mice at one month, three months, and six months of age. When observing the myelin pattern in the cerebellum, there were small areas lacking the blue myelin stain in the *Plp1dup* mice (figure 3.12) when compared to the wild-type. A few holes similar to

those seen within the corpus callosum of the six month *Plp1dup* mouse sections were also observed in the cerebellum. These holes were also present, but in lower numbers, at one and three months. At one month, no difference in the smooth myelin pattern was observed in the *Plp1dup* mice compared to wild-type mice, but the holes were observed within myelin (figure 3.12a). At three months slightly more difference in the white matter tracks of the cerebellum was observed (figure 3.12b). More holes were seen within the white matter tracks and there were a few areas lacking myelin as shown by small areas of missing blue stain in the *Plp1dup* mice when compared to the wild-type. Finally, the six month sections, figure 3.12c, shows more differences between wild-type and *Plp1dup* mice by having more areas of myelin lacking in the cerebellum with the holes throughout the myelin tracks.

To assess whether myelin stability was affected by the duplication in *Plp1* locus, spinal cord myelin from six month *Plp1dup* mice were analyzed by electron microscopy (EM) and compared to six month wild-type mice. Figure 3.13 shows representative data from these analyses and many abnormalities were observed in the *Plp1dup* mice sections. Figure 3.13b shows a degenerating axon (Ax with arrow) that was engulfed by a microglial cell (MG), including astrogliosis (AG) in the *Plp1dup* mice. Figure 3.13c shows a degenerating fiber (DF). Figure 3.13d shows more degenerating fibers (arrows). Figure 3.13e and f show unmyelinated axons (Ax) next to paranode/internode (arrow with PN/IN). These EM images show major abnormalities within the spinal cord myelin in the *Plp1dup* mouse.

EM on the brains of the mice would help acquire a higher resolution and magnification of myelin compaction and stability in the *Plp1dup* mice. Since brain is a large and complex tissue, it is difficult to find specific regions of interest in the brain with EM because this type of microscopy is at such high magnification. Therefore, correlative microscopy will be used to overcome these difficulties. The Bio-Imaging center at University of Delaware helped to map specific regions of the brain by first using a tile scan technique with confocal microscopy to obtain a full image of the brain section. Still using confocal microscopy, the magnification was increased to identify specific regions of interest and coordinates were obtained by identifying unique areas in the section for EM analysis. This will allow images to be obtained of the corpus callosum and cerebellum at a higher magnification observed in the histological experiments.

Preliminary mapping experiments were completed, and so far the confocal steps of the correlative microscopy were started. Using sagittal sections of the brain, areas of the corpus callosum where axons were seen in cross section were used to assess whether myelin compaction and stability was disrupted in this specific region of the brain. Figure 3.14 shows results of the first mapping experiment with six month wild-type and *Plp1dup* mice. Using confocal microscopy, tile scans were performed to obtain a full image of the whole section of the brain (figure 3.14a and d) to help map specific regions of interest. Figure 3.14b and e show second tile scan of a specific region selected from the first tile scan at an increased magnification. Finally, figure

3.14c and f shows a region from the previous panel with increased magnification. These images will next be used to define EM coordinates. Figure 3.14 shows the preliminary work of the mapping experiments. Differences between the wild-type and *Plp1dup* can be observed in this figure, but the data are preliminary, so conclusions cannot be made from these images. However, this mapping will allow specific regions of the brain to be examined by EM to show detail about the disruption of myelin content in the *Plp1dup* mouse brain

Table 3.1 Validation of duplication by capillary electrophoresis of multiplex PCR, analysis of gel in figure 3.1b.

Genotyping Analysis				
DNA	<u>PLP¹:DMD²</u>	<u>neo³:DMD²</u>	<u>region x⁴:DMD²</u>	<u>puro⁵:DMD²</u>
Pup 1	1.09		1.21	
Pup 2	1.87	0.67	2.04	1.02
Pup 3	0.93		1.02	
Pup 4	1.97	0.92	1.84	0.90
Pup 5	1.95	1.12	2.29	1.14
<i>Plp1</i> dup Male Ctrl	2.00	1.09	2.16	1.08
<i>Plp1</i> dup Male Ctrl	1.90	0.91	1.87	0.92
Wild type Male Ctrl	0.96		0.89	
Wild type Male Ctrl	1.04		1.11	

Blue highlighting: *Plp1*dup mouse

¹Region of the *Plp1* amplified using the mPLP-F6 and mPLP-R1 primer pair.

²Region of the *Dmd* amplified using the mDMD28-F and mDMD28-R primer pair.

³Region of the *neo* gene amplified using the neo-F and neo-R primer pair.

⁴Region on the proximal end of the duplication (region x) amplified using the 197O15-F and 197O15-R primer pair.

⁵Region of the *puro* gene amplified using the MHPP-F14 and MHPP-R5 primer pair.

Sequences of these primer pairs are found in table 2.1.

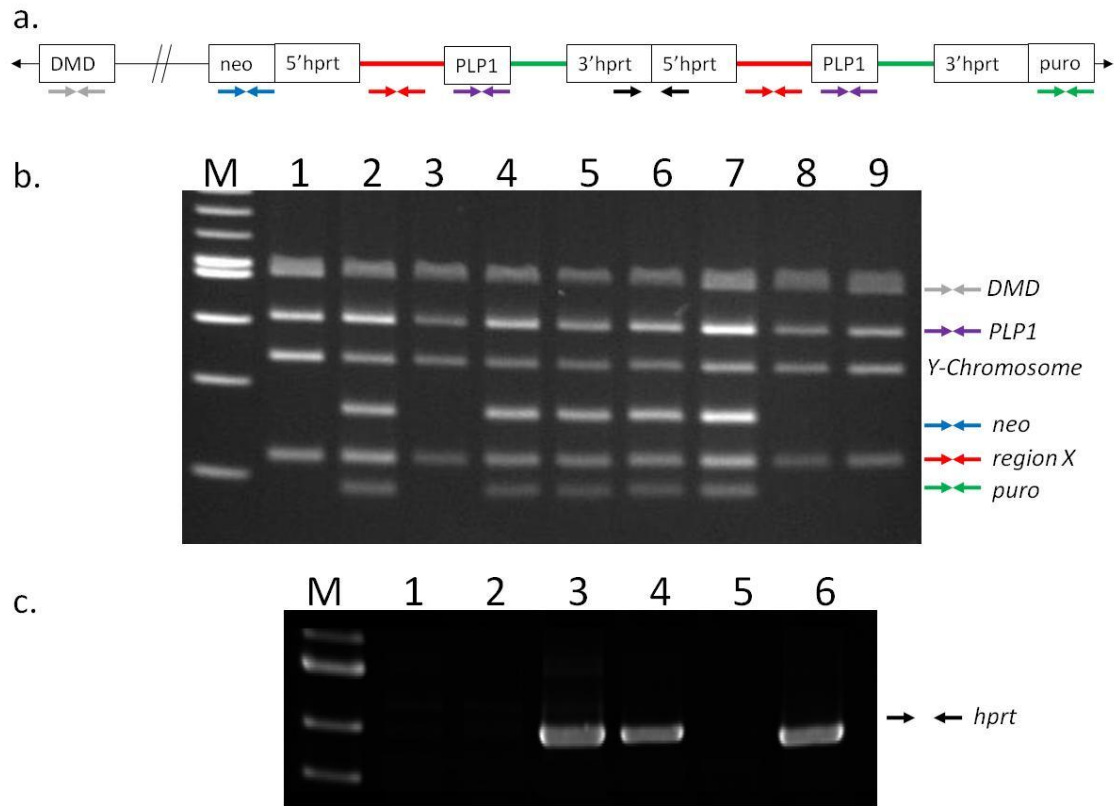


Figure 3.1 Validation of duplication by semi-quantitative multiplex PCR and by amplification across *hprt* gene **a.** Diagram of the duplication that was generated in the *Plp1*dup mouse. Horizontal arrows: positions of the PCR primers, //: large space between *neo* and *DMD* gene, thick red line: duplicated portion proximal of *Plp1*, thick green line: duplicated portion distal of *Plp1* **b.** Sample genotype analysis by multiplex PCR amplification of spleen DNA from a litter of five male mice. Separation of products by agarose gel electrophoresis was used to verify amplification before subjecting samples to capillary electrophoresis. The quantitative data for this gel was obtained by capillary electrophoresis and are shown in table 3.1. Lane M: 100bp marker, lanes 1-5: male pups from a litter, lanes 6 and 7: male controls with the duplication, lanes 8 and 9: wild-type male controls. **c.** Sample genotype analysis by amplification across the *hprt* gene. PCR products were separated by agarose gel electrophoresis. Results indicate that samples in lanes 3 and 4 are from *Plp1*dup male mice, while samples in 1,2, and 5 are wild-type. Lane M: 1kb marker, lanes 1-5: samples from a litter of five male pups, lane 6: normal human DNA control. Grey arrows: represent mDMD28-F and mDMD28-R primer pair, purple arrows: represent the mPLP-F6 and mPLP-R1 primer pair, blue arrows: represent the neo-F and neo-R primer pair, red arrows: represent the 197O15-F and 197O15-R primer pair, green arrows: represent the MHPP-F14 and MHPP-R5 primer pair, black arrows: represent the hHPRT-F2 and hHPRT-R primer pair. All primer pair sequences found in table 2.1.

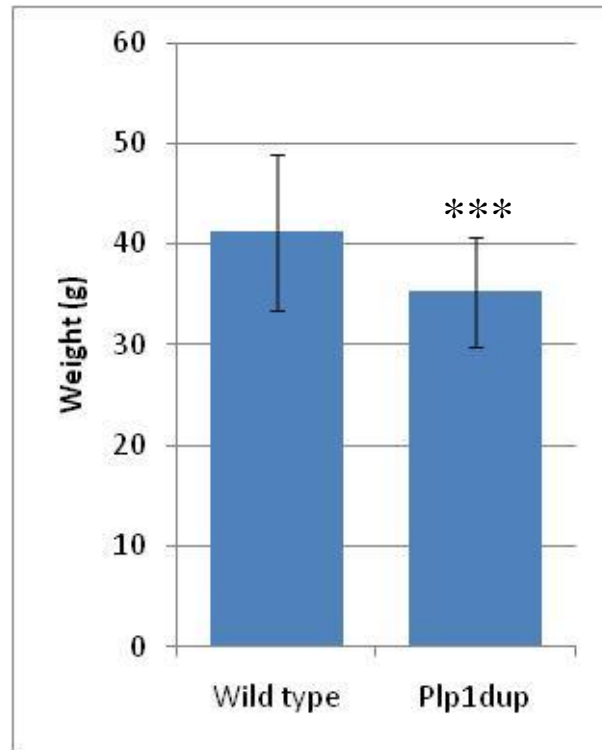


Figure 3.2 Weight difference in *Plp1dup* males compared to wild-type males at six months of age. Results of the quantitative data for *Plp1dup* (n=30) show that they weigh an average of 35.2 grams and wild-type (n=30) males weigh an average of 41.2 grams. *Plp1dup* mice weigh approximately 6 grams less than wild-type males (***, $P < 0.001$).

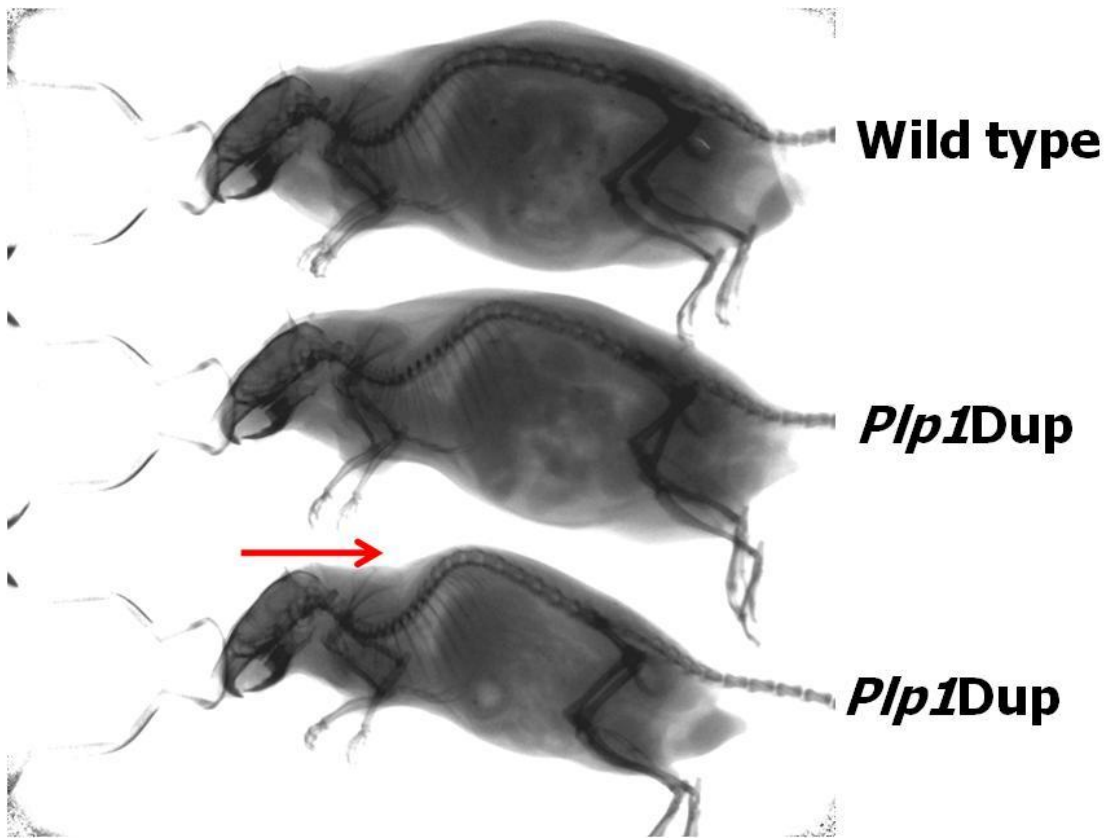


Figure 3.3 X-ray analysis of the *Plp1dup* five month old male mice. The curvature of the spine felt along the spine of *Plp1dup* mice was analyzed by X-ray analysis of *Plp1dup* and wild-type males in these three animals. Red arrow points out the curvature of the spine that is observed in one *Plp1dup* mouse and has not been felt in wild-type mice. The curvature was not felt in the first *Plp1dup* mouse in this figure and it was not seen in the X-ray.

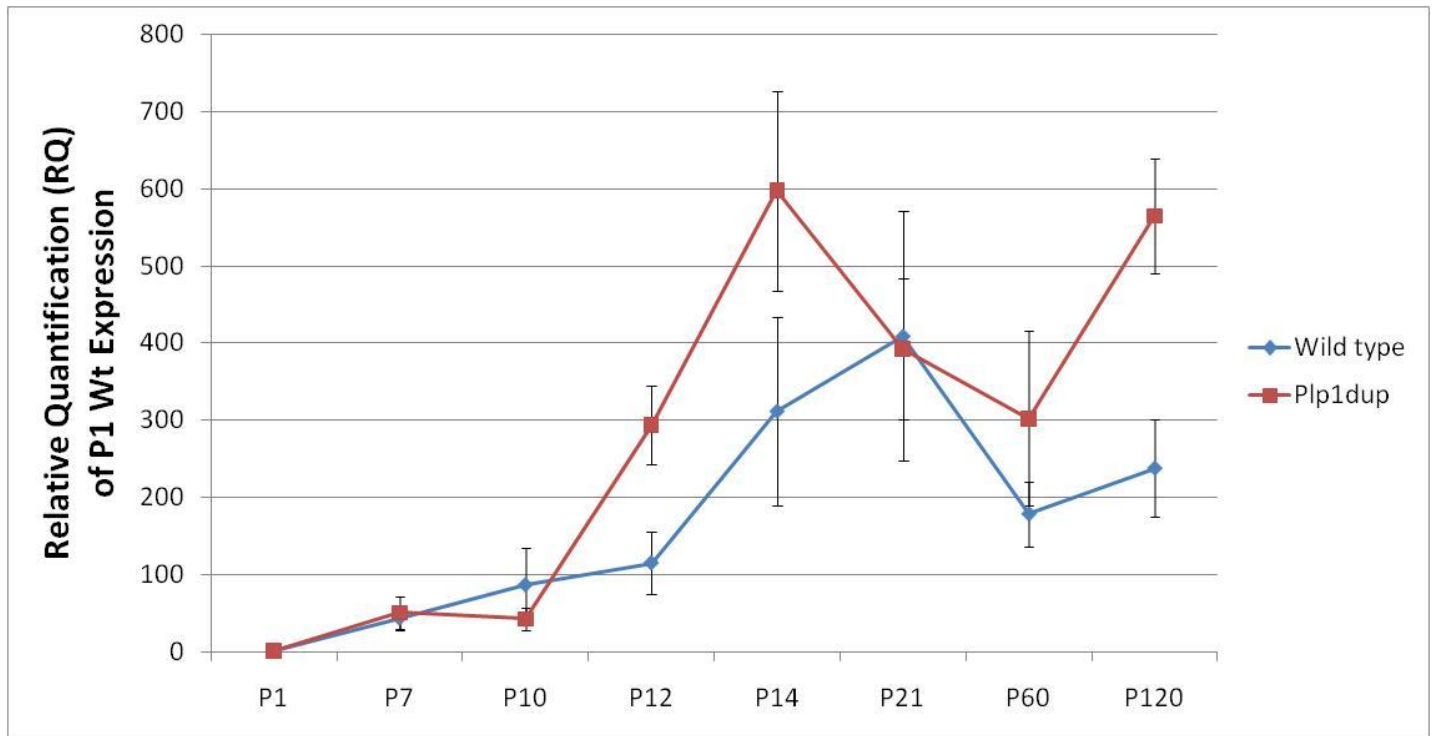


Figure 3.4 Developmental profile of *Plp1+Dm20* mRNA expression in *Plp1dup* and wild-type mouse brain. The quantitative data shown over the developmental time set for *Plp1+Dm20* mRNA expression relative to P1 wild-type. Data were measured by real time qRT-PCR of total RNA isolated from *Plp1dup* (n=3) and wild-type (n=3) mouse brain at each time point. Results show a triphasic expression pattern in the wild-type animals, with a different expression pattern seen in the *Plp1dup* mice. These data show an overexpression of *Plp1+Dm20* from P12 to P120 with a regulation to normal levels at P21 in the *Plp1dup* mice.

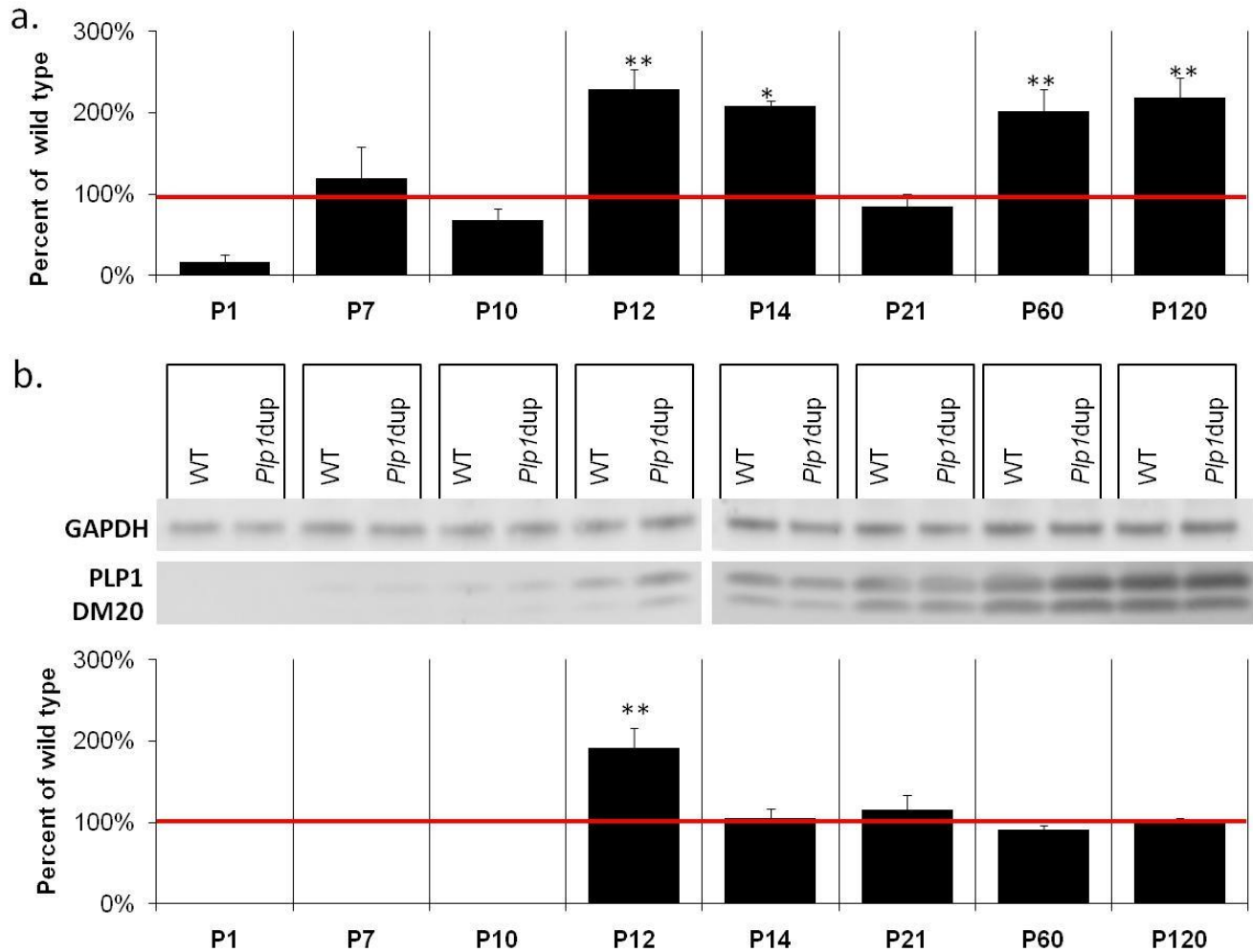


Figure 3.5 Altered expression of *Plp1+Dm20* mRNA and PLP1+DM20 protein in *Plp1dup* relative to wild-type mice. **a.** Quantitative data for *Plp1+Dm20* mRNA expression in brain measured by real time qRT-PCR of *Plp1dup* (n=3) and wild-type (n=3) males at each time point indicated. Results were expressed as a percentage of the average of three wild-type mice. P1, P7, P10, and P21 show no difference from wild-type, but significant increases were observed in *Plp1dup* mice at P12, P14, P60, and P120. **b.** Quantitative data for PLP1+DM20 protein measured from the Western blot. Results for the *Plp1dup* mice (n=3) were expressed as a percentage of wild-type (n=3) protein expression. Elevated PLP1+DM20 levels were observed in the *Plp1dup* at P12, but wild-type levels were observed at older ages. A representative Western blot is shown above the graph. Protein homogenates were prepared from brain at postnatal days indicated. The blot was probed with antibody that recognizes PLP1 and DM20 and an antibody to GAPDH as a loading accuracy control (*p < 0.05, **p < 0.01).

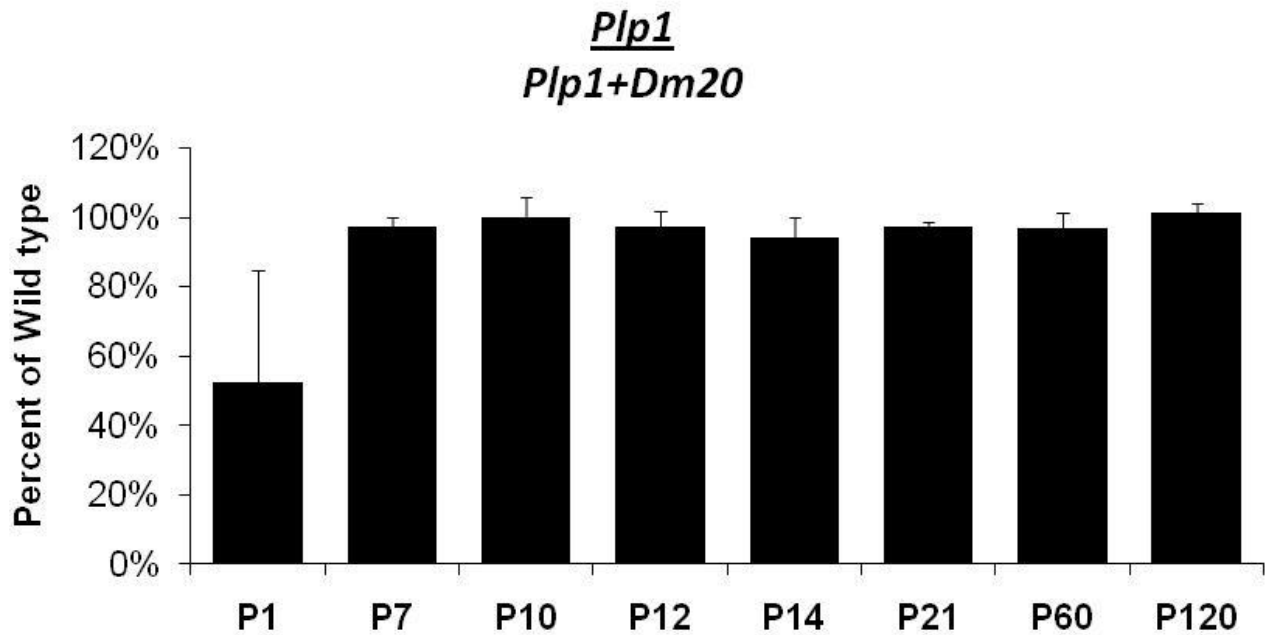


Figure 3.6 *Plp1* and *Dm20* alternatively spliced transcript levels in the *Plp1dup* are similar to wild-type. Quantitative data for the ratio of the *Plp1* isoform over *Plp1+Dm20* mRNA expression in the *Plp1dup* compared to wild-type levels. The levels of alternative spliced products *Plp1* and *Dm20* were similar in the *Plp1dup* mice compared to wild-type controls.

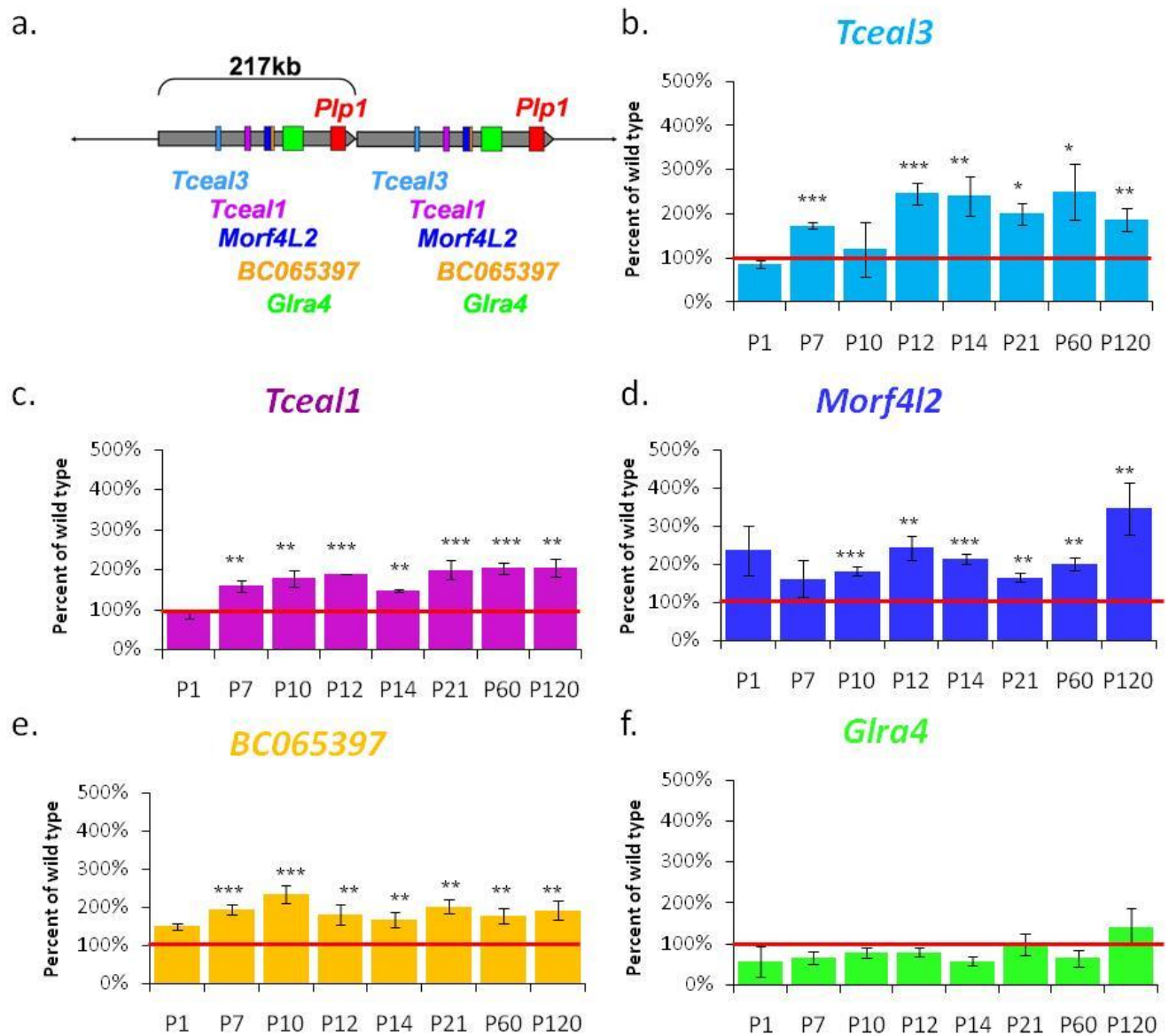


Figure 3.7 Altered mRNA expression of the genes within the duplication, other than *Plp1*, in *Plp1dup* mice relative to wild-type mice. **a.** Diagram of the duplication showing the location of the other genes found within the duplication relative to *Plp1*. Quantitative data for **b.** *Tceal3* **c.** *Tceal1* **d.** *Morf4l2* **e.** *BC065397* and **f.** *Glr4* mRNA, measured by real time qRT-PCR of mRNA from brain at the time points indicated from *Plp1dup* (n=3) and wild-type (n=3) male mice. Results are expressed as a percentage of wild-type mice, and elevated levels of mRNA for all genes was observed in *Plp1dup* mice compared to wild-type mice except for *Glr4* (*p < 0.05, **p < 0.01, and ***p < 0.001).

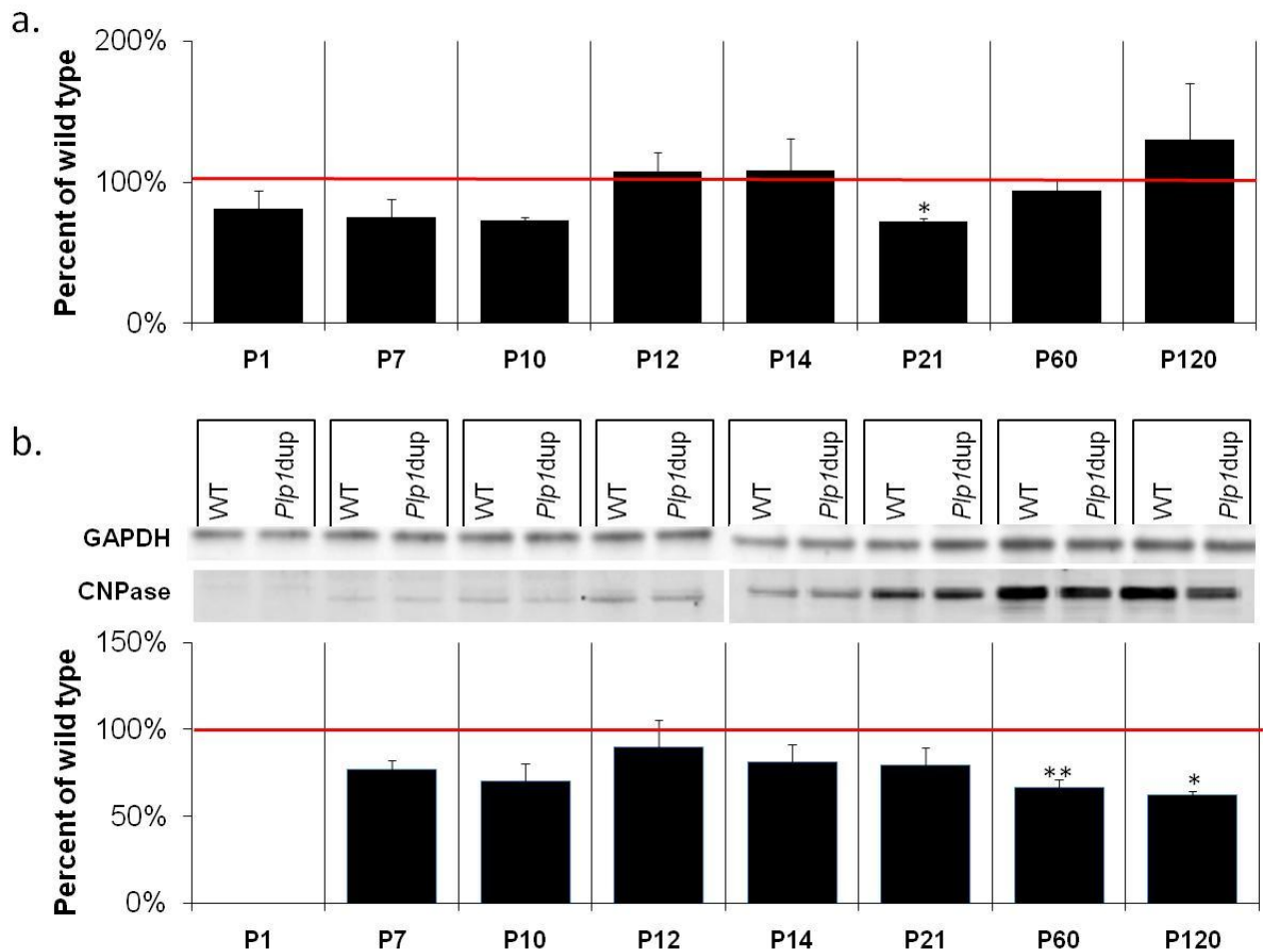


Figure 3.8 Close to wild-type expression levels of CNPase mRNA over the developmental set with lower protein levels in adult *P1pl1dup* mice compared to wild-type mice. **a.** Quantitative data for CNPase mRNA, measured by real time qRT-PCR of RNA from brain at the time points indicated for *P1pl1dup* (n=3) and wild-type (n=3) male mice. Results are expressed as a percentage of wild-type mice. There was only a difference observed in the *P1pl1dup* mice compared to wild-type at P21 when a slightly lower amount of CNPase expression in the *P1pl1dup* mice was observed. **b.** Quantitative data for CNPase protein measured from the Western blot. Results for the *P1pl1dup* mice (n=3) are expressed as a percentage of wild-type (n=3). Lower CNPase protein levels were observed in the *P1pl1dup* mice at P60 and P120. A representative Western blot is shown above the graph. Protein homogenates were prepared from brain at postnatal days indicated. The blot was probed with antibody to CNPase and an antibody to GAPDH as a loading accuracy control (*p < 0.05 ** < 0.01).

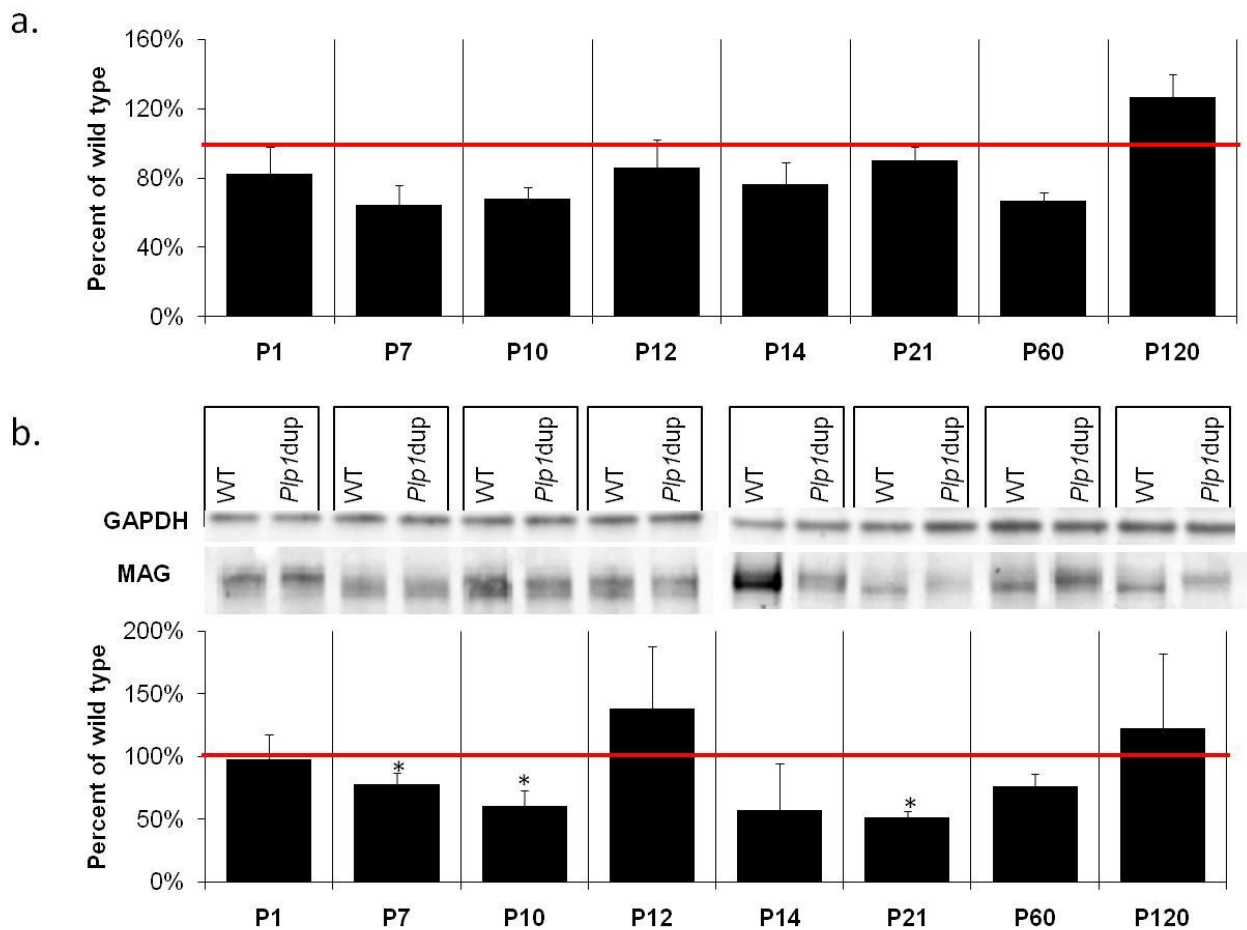


Figure 3.9 Wild-type levels of MAG mRNA expression with altered protein levels in the *Plp1dup* mice compared to wild-type mice. a. Quantitative data for *Mag* mRNA, measured by real time qRT-PCR of RNA from brain at the ages indicated of *Plp1dup* (n=3) and wild-type (n=3) male mice. Results are expressed as a percentage of wild-type mice. There is no significant difference observed in the *Plp1dup* mice compared to wild-type over the developmental set. **b.** Quantitative data for MAG protein measured from the Western blot. Results for the *Plp1dup* mice (n=3) are expressed as a percentage of wild-type (n=3). Lower MAG protein levels were observed in the *Plp1dup* at P7, P10 and P21. A representative Western blot is shown above the graph. Protein homogenates were prepared from brain at postnatal days indicated. The blot was probed with antibody to MAG and an antibody to GAPDH as a loading accuracy control (*p < 0.05).

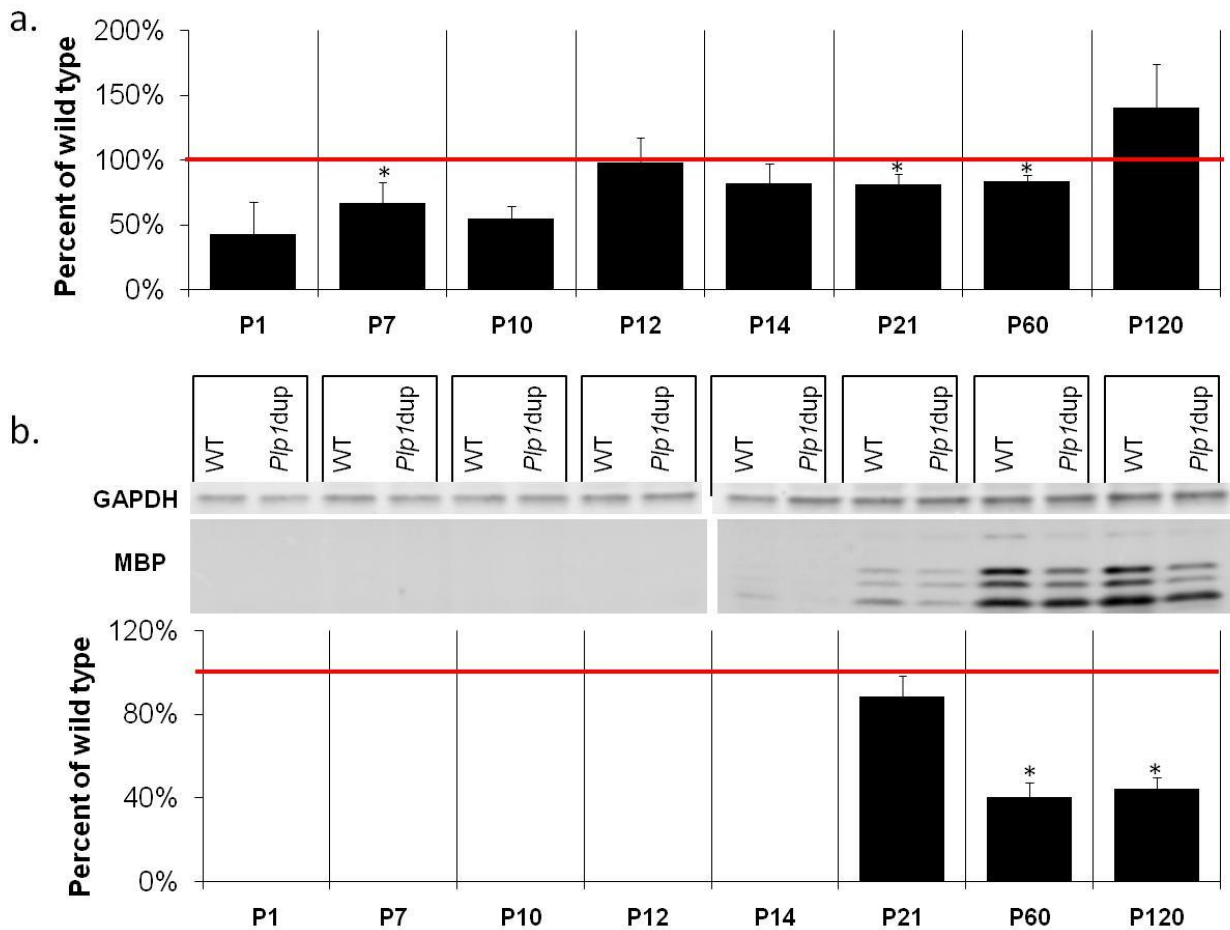


Figure 3.10 Lower levels of MBP mRNA and protein expression in the *Plp1dup* mice compared to wild-type mice. a. Quantitative data for *Mbp* mRNA, measured by real time qRT-PCR of RNA from brain at the ages indicated of *Plp1dup* (n=3) and wild-type (n=3) male mice. Results are expressed as a percentage of wild-type mice. There were slightly lower levels observed in the *Mbp* mRNA expression in the *Plp1dup* mice compared to wild-type at P7, P21, and P60. **b.** Quantitative data for MBP protein measured from the Western blot. Results for the *Plp1dup* mice (n=3) are expressed as a percentage of wild-type (n=3). MBP protein begins to be expressed at P20, and lower MBP levels are observed in the *Plp1dup* at P60, and P120. A representative Western blot is shown above the graph. Protein homogenates were prepared from brain at postnatal days indicated. The blot was probed with antibody to MBP and an antibody to GAPDH as a loading accuracy control (*p < 0.05).

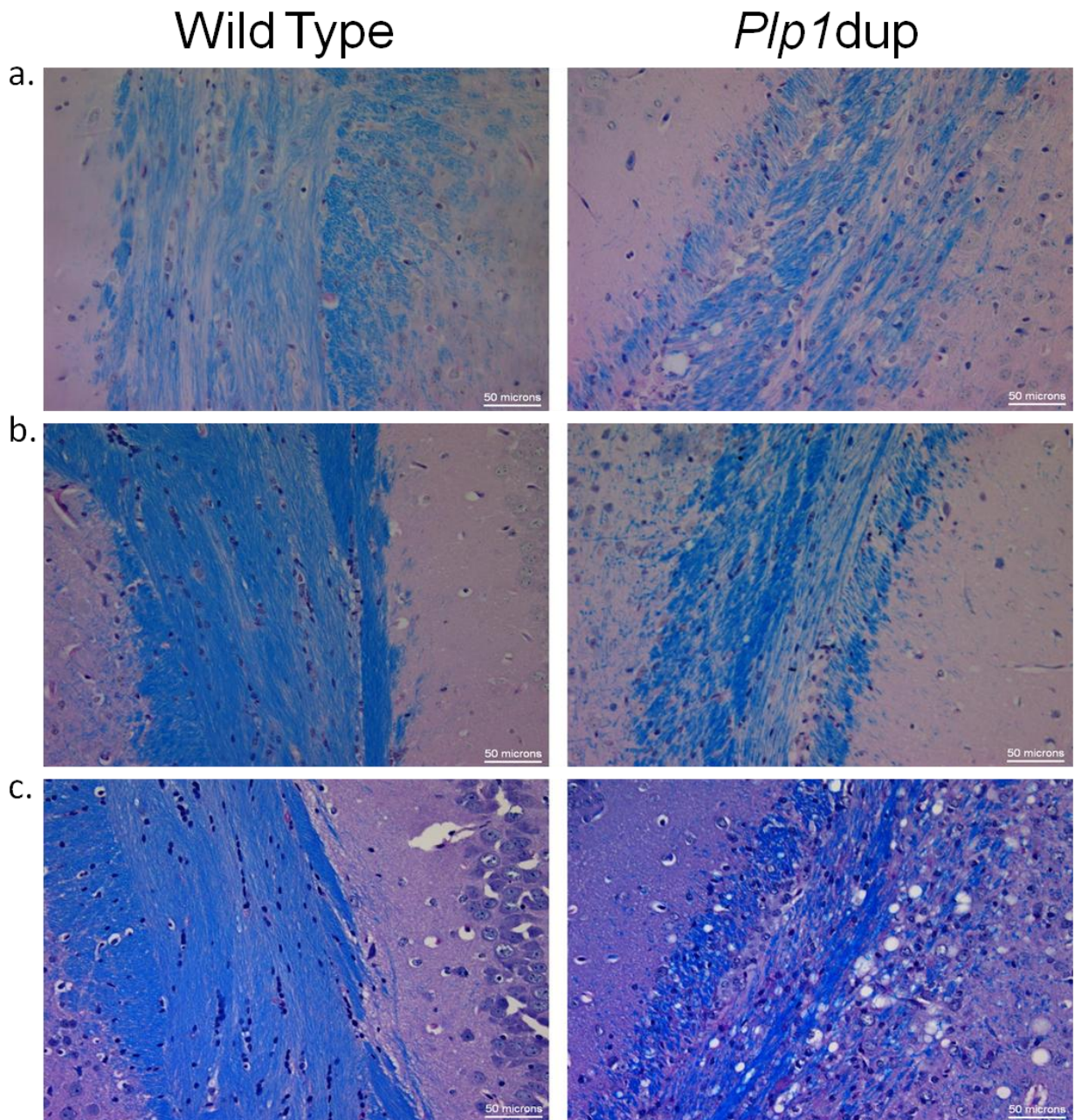


Figure 3.11 Discontinuous myelination pattern in the corpus callosum of *Plp1dup* mice. Representative image of 5 μ m thick brain sections of **a.** one month, **b.** three month, and **c.** six month wild-type and *Plp1dup* mice stained with Luxol-Fast Blue and PAS. Results show a discontinuous pattern of myelin (blue stain) in the corpus callosum in the *Plp1dup* mouse compared to the wild-type pattern (n = 3). Holes were observed along myelination pattern in the six month *Plp1dup* mice. Scale bar: 50 microns.

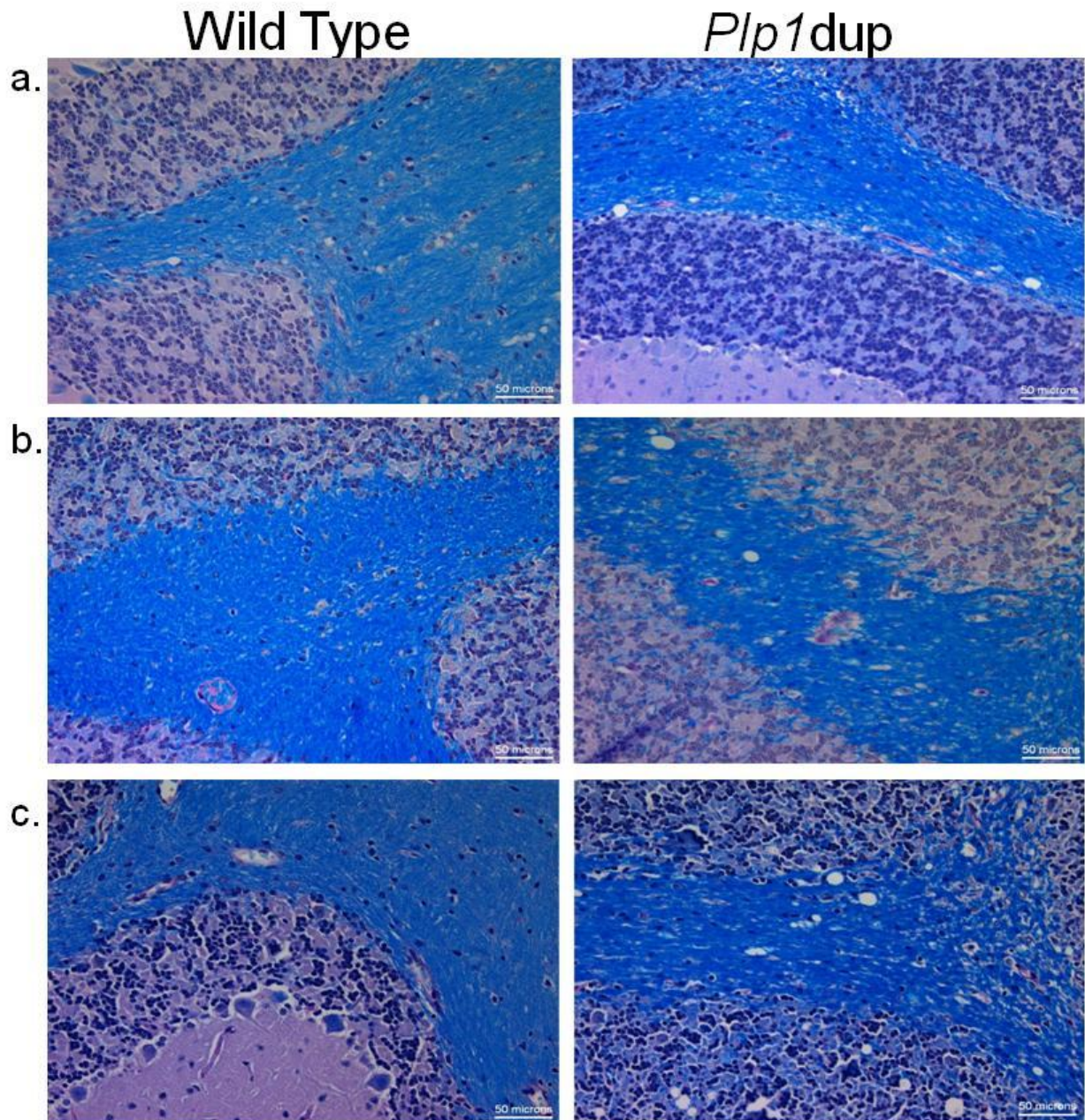


Figure 3.12 Discontinuous myelination pattern in the white matter tracks of the cerebellum of *Plp1dup*. Representative image of 5 μ m thick brain sections of **a.** one month, **b.** three month, and **c.** six month wild-type and *Plp1dup* mice stained with Luxol-Fast Blue and PAS. Results show a slight discontinuous pattern of myelin (blue stain) in the cerebellum white matter tracks in the *Plp1dup* (n = 3) compared to the wild-type (n = 3) myelin pattern. In *Plp1dup* mouse brain holes were observed along myelination pattern also. Scale bar: 50 microns.

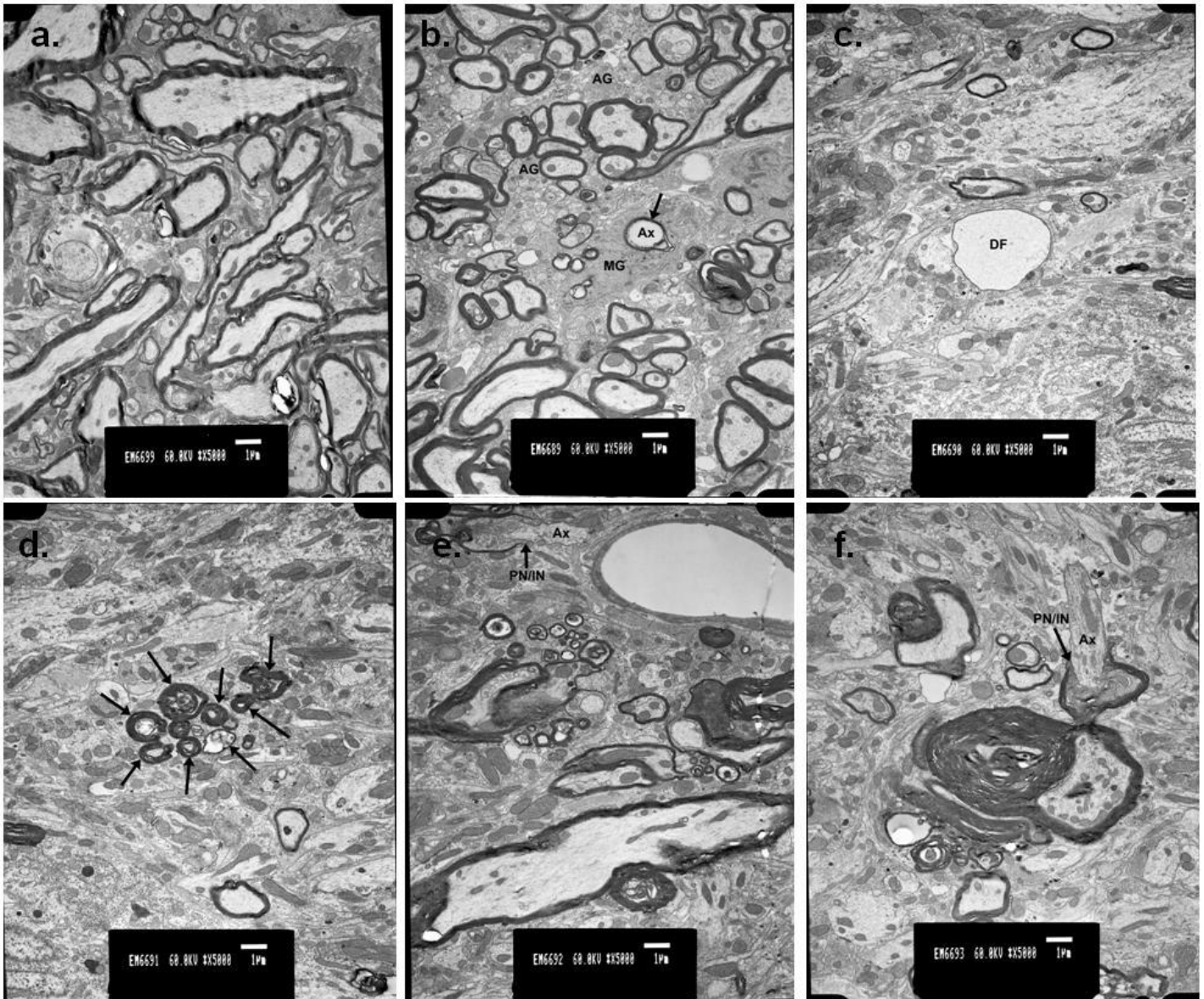


Figure 3.13 Disruption of normal myelin formation in *Plp1dup* spinal cord.

Representative electron micrographs of spinal cord of six month mice **a.** Wild-type mouse **b.** *Plp1dup* mouse with a degenerating axon (Ax w/ arrow) engulfed by a microglial cell (MG) showing astrogliosis (AG) **c.** *Plp1dup* mouse showing degenerating fibers (DF) **d.** *Plp1dup* mouse showing degenerating fibers (arrows) **e.** *Plp1dup* showing an unmyelinated axon (Ax) next to paranode/internode (arrow w/ PN/IN) **f.** *Plp1dup* mouse showing an unmyelinated axon (Ax) next to paranode/internode (arrow w/ PN/IN). Scale bar: 1 micron.

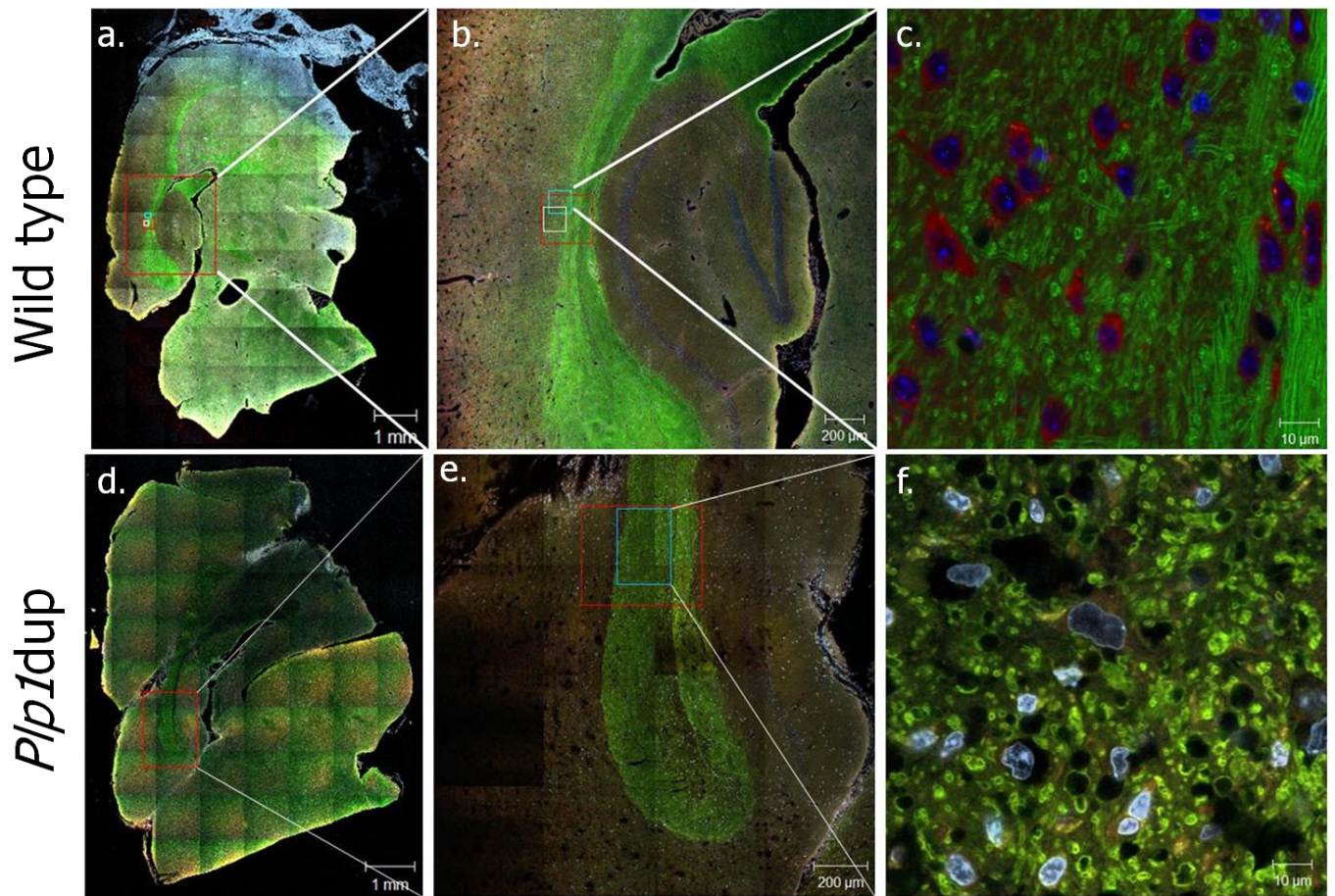


Figure 3.14 Preliminary data indicating how specific regions of the brain will be mapped for electron microscopy using confocal microscopy. Images of brain sections of **a. - c.** six month wild-type and **d. - f.** six month *Plp1dup* mice stained with Brain Stain. **a. and d.** Show the tile scanning technique using a 10x/0.45 objective lens. Images of 15 x 15 were tiled to form a full image. **b. and e.** Show zoomed into the red square at corpus callosum taken with 10x/0.45 objective at 1-fold zoom and captured 5 x 5 images then tiled to form a full image. **c. and f.** Show a 2-fold zoom into the blue square of an area of interest showing cross sections of myelin (green) using 10x/0.45 objective. Specific regions of brain will be located and targeted for TEM using this method. Green: fluorescent myelin stain, Red: fluorescent Nissl stain (cell bodies), Blue: DAPI dihydrochloride (DNA).

Chapter 4

DISCUSSION

Duplication of the *Plp1* locus that includes the entire *Plp1* gene is the most frequent cause of PMD. Existing transgenic rodent models containing extra copies of *Plp1* have been characterized, but none of these exactly replicated what is most commonly found among PMD patients. This is the first report of a model that is genetically similar to PMD patients by containing a 217 kb tandem genomic duplication of the X chromosome that not only contains *Plp1*, but adjacent DNA. Thus, the duplication also includes regulatory regions as well as five other neighboring genes. Our new model, the *Plp1dup* mouse, is a more accurate representation of the human duplication at the *Plp1* locus that causes PMD compared to previously used models. Conclusions from the characterization of this new mouse model were that the duplication in the *Plp1* locus altered the expression of the genes within the duplication, including *Plp1*. Change in *Plp1* expression leads to altered expression of major myelin proteins and disruption of normal myelin formation, which is similar to PMD patients.

The experiments presented in this thesis were performed on a C57BL/6J and 129S1/SvImJ mixed background mouse line. This mixed background line leads to variation from mouse to mouse due to genetic differences from the two

different backgrounds. The mixed background mice makes the data reported here more like what may be observed in a human population, which has a much higher genetic variability. However, the mixed background could account for some of the large error bars and variation from mouse to mouse that was seen in the X-ray analysis (figure 3.3) and protein expression of MAG (figure 3.9b). Increasing sample size could eliminate some of the error observed in the mixed background line. Our lab is currently working on reproducing this work on a congenic line of C57BL/6, thus allowing for the only difference between the *Plp1dup* and wild-type mice to be the duplication in the *Plp1* locus.

The duplication leads to a distinct abnormal phenotype. An abnormal phenotype was observed in mice during simple weaning and other handling activities. For instance, *Plp1dup* mice display problems lifting up their body when being held by their tail, as compared to wild-type litter mates. The data suggest that the duplication causes a development of a curvature in the spine (figure 3.3) and causes noticeable weight difference (figure 3.2). Both slow growth and skeletal deformation are symptoms that have been reported in PMD patients. To determine whether the observed curvature of the spine is due to neuromuscular or skeletal defects, all of the soft tissues must be removed to visualize the spine without influence from the muscle. Later in life, the *Plp1dup* mice develop seizures more often than wild-type mice at approximately one year of age. However, only seven *Plp1dup* mice and seven wild-

type littermates were kept until they were a year old. Our lab is currently working to obtain quantitative data on the seizure phenotype.

Previously, it was presumed that *Plp1* duplications cause disease as a result of an overexpression of *PLP1*, but this has not yet been confirmed in patients with PMD (Anderson et al., 1998; I. Griffiths et al., 1998; Karim, Barrie, McCulloch, Montague, Edgar, Kirkham, Anderson, Nave, Griffiths, & McLaughlin, 2007). Characterization of the *Plp1*dup mouse confirms this might be true, but with a much greater complexity than originally thought. The duplication in the *Plp1* locus results in an overexpression of *Plp1* transcripts in the brain, but not until P12 and older. Interestingly, at the peak of myelination, P21, there must be a transcriptional or post-transcriptional regulation that keeps specific mRNA levels at P21, so even with a duplication in the *Plp1* locus the levels are the same. Results from this report confirmed what was previously shown (Kanfer et al., 1989), that *Plp1* displays a triphasic mRNA expression pattern in wild-type mice; a gradual increase in the level of *Plp1* transcript leading to a peak at P21, and this is followed by a decline to a plateau level. It is thought that neuronal signals are responsible for the increased level of myelin related mRNA such as *Plp1* (Kanfer et al., 1989). An important regulation at the peak of myelination may cause mRNA levels to be tightly controlled, thus regulating *Plp1* mRNA levels to a set amount, even with an increased gene dosage, as observed at P21 in figure 3.4 and 3.5a. Understanding how *Plp1* mRNA is regulated at this stage is important mechanism that needs to be elucidated.

Terminal complement complexes play a role in the inflammatory pathway and could play an important role in regulating important myelin proteins at a post-transcriptional level if there is activation of the complement system's terminal pathway. This could be one possible explanation for the mRNA levels observed in the *Plp1*dup mice. The effect of terminal complement complexes in oligodendrocytes on myelin protein gene expression was published, although terminal complement complexes are best known insert into a target as membrane attack complex (MAC) causing cytolysis (Dobrina et al., 2002). Recent evidence has proved that terminal complement complexes in sublytic amounts can have noncytolytic effects on several target cells. Results have specifically shown that sublytic activation of serum C reduced accumulation of mRNA encoding *Plp1* and *Mbp* (Shirazi, Rus, Macklin, & Shin, 1993). If there is an inflammatory process in the *Plp1*dup mice due to an overexpression of *Plp1*, then *Plp1* mRNA could be post-transcriptionally regulated explaining that even with an extra gene dosage of *Plp1* mRNA levels can be down-regulated to normal levels, as seen at P21 (figure 3.4 and 3.5a). The microglial cells that were shown engulfing the degenerating axons in the spinal cord (figure 3.13b) supports the hypothesis that an inflammatory response could be occurring in *Plp1*dup mice since these macrophages are the first immune defense in the CNS.

Even though the *Plp1* mRNA levels were altered in the brain of mice with a duplication in the *Plp1* locus, no change was observed in the *Plp1/Dm20* alternative splicing ratio (figure 3.6). This data does not agree with what was previously reported,

that a gene duplication causes alteration of the *PLP1* to *DM20* splicing balance in cultured skin fibroblasts from patients with PMD (Regis et al., 2009). The findings in the *Plp1*dup mice are not unusual because *Plp1* expression was analyzed in brain where it is highly expressed. Only low levels of *PLP1+DM20* are expressed in fibroblasts and the ratios obtained from this tissue may be misleading due to the small volume.

PLP1+DM20 protein was overexpressed when the protein was first detected at P12, but after that, the same PLP1+DM20 protein expression levels were seen whether the duplication was present or not. In the #66 hemizygous mouse with seven extra copies of *Plp1*, it was reported that in spinal cord there was an increase in protein levels at P3 and normal levels at P20 (Karim, Barrie, McCulloch, Montague, Edgar, Kirkham, Anderson, Nave, Griffiths, & McLaughlin, 2007). These results are similar to the pattern seen in the *Plp1*dup mouse, where at early protein expression, P12, there is an overexpression of PLP1+DM20 protein and normal levels at P14, P21, P60, and P120 (figure 3.5b). The level of PLP1 that is released and inserted into the myelin is a controlled process, and this control could be attributed to translational regulation, rapid turnover, or degradation which explains wild-type protein levels when a duplication exists in the *Plp1* locus (Karim et al., 2010).

Results in this report support the idea previously published that PLP1 is highly translationally regulated. It was previously published that the rate of PLP1 translation is decreased in homozygous (14 copies of *Plp1*) #66 line (Karim et al.,

2010). The idea that miRNA could influence PLP1 translation was suggested. This miRNA regulation has shown to be important in the translation of PMP22, which is a peripheral myelin protein that is overexpressed in Charcot-Marie-Tooth disease type 1A (Karim et al., 2010; Verrier et al., 2009). The mouse model characterized in this thesis only provides evidence that supports the hypothesis of translational control since the levels of *Plp1* mRNA are shown to be increased due to the genomic duplication, but normal protein levels are observed except at P12, the earliest time of detection.

This report also supports the hypothesis that PLP1 is regulated at the post-translational level. In wild-type oligodendrocytes, approximately 30% of newly synthesized PLP1 is degraded by proteasomes (Karim et al., 2010). This is the same process that has shown to be important in degrading the misfolded PLP1 (McLaughlin et al., 2006). Twice as much PLP1 (approximately 60%) was subject to degradation by this process in oligodendrocytes derived from homozygous (14 copies of *Plp1*) #66 mouse line compared to the wild-type when degradation was measured by a pulse-chase assay (Karim et al., 2010). The structure of PLP1 in the #66 homozygous mice is thought to be identical to wild-type protein, and therefore does not activate the misfolded protein response. The amount of PLP1 protein inserted into myelin in #66 homozygous mice is about a third of that incorporated in wild-type, so the extra PLP1 is thought to be degraded (Karim et al., 2010). This hypothesis of PLP1 protein regulation through proteosomal degradation could explain the results in the current report, that at an early developmental time point during myelination PLP1 protein was

increased compared to wild-type due to increased gene dosage, and this excess PLP1 leads to the later degradation of all the excess protein by proteosomes. Thus, degradation leads to normal PLP1 protein levels at P14, P21, P60, and P120 even with a duplication in the *Plp1* locus.

The translational and post-translational regulation hypothesis should be further studied in the *Plp1dup* mouse. As seen in table 1.1, the previous mouse models were only analyzed at a single time point and showed that PLP1 is either overexpressed or underexpressed usually dependent upon whether they are hemizygous or homozygous. In the *Plp1dup* mouse model, the duplication is similar to what patients will have, and the developmental expression pattern of PLP1 during myelination was observed in this report showing its complex expression (figures 3.4 and 3.5), and a greater understanding of PLP1 regulation could be elucidated using this model. It is possible that the duplication alters the regulation and insertion of PLP1 into the myelin. In order to determine this, a localization assays must be performed in the *Plp1dup* mouse to visualize if PLP1 is inserted into myelin or is elsewhere in the cell. Since results in this study show that PLP1 protein levels are regulated to wild-type levels during myelination and into adulthood, it is important to elucidate the location of this protein to understand the improper formation of myelin seen in figures 3.11, 3.12, and 3.13. There is a regulation allowing for the proper amount of PLP1 protein in whole brain, but the issue might exist in the regulation of the PLP1 protein being properly inserted into the myelin.

Timing of the myelin development could be crucial and is yet another explanation of the improper myelin formation observed in the *Plp1dup* mice. In wild-type mice, the peak of myelin accumulation is at P21, and this is also where *Plp1* expression reaches a peak (Kanfer et al., 1989). However, in the *Plp1dup* mice *Plp1* expression reaches a peak at an earlier age, P14 (figure 3.4), and this could be detrimental to proper myelin formation. The lab will have to investigate myelin formation by measuring the accumulation of myelin, then it could be identified if myelin is reaching a peak accumulation at an earlier time in the *Plp1dup* mice. If this timing of myelin formation is occurring sooner, this could be cause the improper formation that was observed in the *Plp1dup* and cause the degeneration and hypomyelination seen in these animals.

Improper myelin formation due to the duplication in the *Plp1* locus could account for the decrease in other myelin proteins: MBP, MAG, and CNPase (Figures 3.8, 3.9, and 3.10). Normally, PLP1 associates with cholesterol and other lipids to form myelin rafts during trafficking through the Golgi complex (Simons et al., 2000). Excessive amounts of PLP1 proteins have been shown previously to disrupt this pathway, and excessive amounts of normal PLP1 protein accumulate in late endosome and lysosomal compartments of rodent cells (Simons et al., 2002). Therefore, overexpression of PLP1 causes an improper transport and assembly of myelin constituents, and would explain the decrease in levels of other myelin proteins and the improper formation of myelin. The holes observed in the pathology experiments could

be where lipids and protein, including excess PLP1, are not being effectively inserted into myelin and are being washed away during processing of the slides. If this hypothesis is true, it would further explain why protein levels of PLP1 are observed to be normal with the duplication, but improper myelin formation is observed.

Interestingly, MBP has slightly lower levels of mRNA expression in the *Plp1*dup mice compared to wild-type mice and a decrease in protein expression due to the duplication. MBP was shown to be the only myelin protein to be essential for formation of CNS myelin (Boggs, 2006). Interactions have been shown to exist between MBP and PLP1 by using a microtitre well binding assay and affinity chromatography, and these studies showed that PLP1 binds to MBP, but not to any other CNS myelin proteins (Edwards, Ross, Ulmer, & Braun, 1989; Wood, Vella, & Moscarello, 1984). It has been shown that MBP influences the partitioning of PLP1 in lipid rafts (Fitzner et al., 2006). When PLP1 is ready for raft formation, a signal transduction cascade could be sent to express MBP to help with the partitioning of these lipid rafts. However, when PLP1 is overexpressed, the excess proteins along with other myelin constituents that normally associate with PLP1 in these rafts are found in the lysosomal and endosomal vesicles. If this raft formation is important in signaling for *MBP*, then it would explain why an increased gene dosage of *Plp1* would cause decreased levels of MBP because it would get degraded in the lysosome and endosomes.

The mRNA expression of MAG and CNPase does not correlate with their protein expression levels in the *Plp1dup* mouse. MAG and CNPase have generally normal mRNA expression levels during myelination into adulthood in the *Plp1dup* mice (figure 3.8 and 3.9). However, CNPase has a significant decrease of protein in the adult *Plp1dup* mouse brain compared to wild-type mice as mice age (figure 3.8b). MAG does not have a simple decrease in expression as mice age like CNPase does, but at P7, P10, and P21 MAG protein is decreased due to an extra dose of *Plp1* (figure 3.9b). This lack of correlation between mRNA and protein expression in MAG and CNPase could be explained by the importance of MBP in the formation of myelin. This report shows that the *Plp1dup* mouse has low mRNA and protein levels of MBP, which could influence the myelin that is formed in these animals since MBP is necessary for myelin formation (Boggs, 2006). This hypothesis could be tested by culturing oligodendrocytes from *Plp1dup* mice and transfect them with an overexpressing vector with MBP to increase the expression of this gene in the *Plp1dup* animals to see if MAG and CNPase levels return to normal.

Since *Plp1* was shown to be sensitive to gene dosage in such a complex way, other genes within the duplicated region might also play a critical role in the phenotype of PMD. The mRNA expression of the five genes other than *Plp1* that are in the *Plp1dup* duplication was analyzed and four of the five were found to be increased about two-fold. *Tceal1*, *Tceal3*, *Morf4l2*, and *Gira4* are commonly found within the duplicated region of patients, so it is important to understand if the function

of these genes is affected by overexpression. *Tceal1*, *Tceal3*, and *Morf4l2* are expressed from 1.5 to 3.5 fold more than wild-type when included in the chromosomal duplication in the *Plp1* locus (figure 3.7). Interestingly, none of the overexpressed genes show normal levels at P21, as seen in *Plp1* (figure 3.5a). This result leads to the hypothesis that there must be a regulation that is specific to *Plp1* transcription at this time point. Although altered expression of *Tceal1*, *Tceal3*, and *Morf4l2* has been reported to be involved with tumors it has not been reported that PMD patients have an increase incidence of tumors. The *Plp1*dup mice also do not develop tumors and we did not detect a phenotype that would be attributed to overexpression of *Tceal1*, *Tceal3*, and *Morf4l2*. However, the fact that an extra dose of these genes could contribute in some way to phenotype in these patients cannot yet be eliminated.

BC065397 is a hypothetical gene that is thought to be part of Ras-like GTPase superfamily, and found at Xq22 in the mouse genome. This hypothetical gene is overexpressed with an extra gene dosage. This hypothetical gene has not yet been reported to be in the human genome, but cannot be ignored when characterizing this new mouse model. Unlike the other duplicated genes, *Gtra4* was not shown to be sensitive to gene dosage (figure 3.7f). In fact, it was previously reported that this gene is not considered to be involved in the phenotype of PMD (Muncke et al., 2004).

Actually, unlike other glycine receptor subunit genes, *Gtra4* harbors a premature stop codon within exon 9, so the forth transmembrane domain is not translated. Thus, *Gtra4* is thought to be a non-functional pseudogene (Muncke et al., 2004).

In conclusion, this study has elaborated on the simple idea that an increased gene dosage of the *Plp1* gene leads to an overexpression of mRNA and protein levels. Interestingly, PLP1 has a complex regulation, leading to not just a simple overexpression due to a genomic duplication, but a complicated altered PLP1 expression throughout the development into adulthood. This model will allow for the study of how, not only *Plp1*, but the neighboring DNA, including the other genes, is important to understanding how this type of genomic duplication leads to PMD. Other genes that have been shown to be overexpressed due to an extra gene dosage exist within genomic duplications found among PMD patients and should be taken into account when trying to understand how a duplication in the *Plp1* locus leads to PMD. The *Plp1*dup mouse model is a more accurate representation of PMD compared to previously reported models and the initial characterizations presented here are the early steps of elucidating the role of a genomic duplication in the *Plp1* locus on the PMD phenotype.

Appendix A

NORMALIZATION OF REAL-TIME RT-PCR

Due to the sensitivity in real-time PCR results, finding the most stably expressed control gene in mouse brain tissue along the developmental time course studied in this thesis was very important. Increasing evidence has been shown that normalizing to a single reference gene introduces large and variable errors into analysis. The geNorm system was used for selecting the best candidate reference genes for the present data in this thesis. The underlying principles and formulas for this system have been described (Vandesompele et al., 2002). The table below shows the 12 reference genes measured with our samples (PrimerDesign).

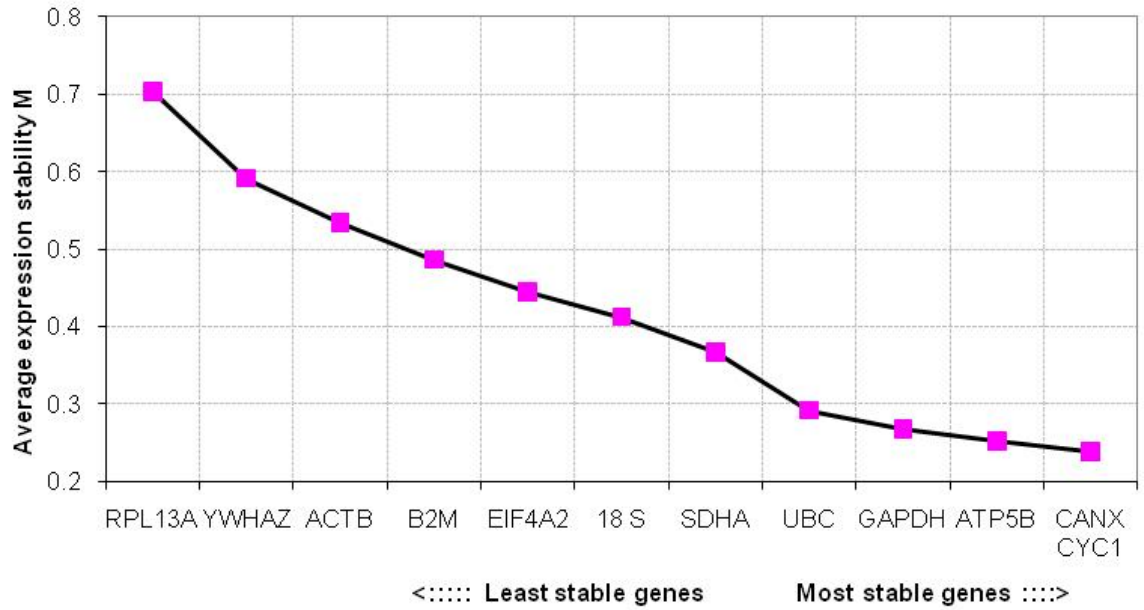
Mouse geNorm reference gene kit	
1	Mus musculus actin, beta, cytoplasmic (ACTB), mRNA.
2	Mus musculus glyceraldehyde-3-phosphate dehydrogenase (GAPDH), mRNA.
3	Mus musculus ubiquitin C (UBC), mRNA.
4	Mus musculus beta-2 microglobulin (B2M), mRNA.
5	Mus musculus phospholipase A2 (YWHAZ), mRNA.
6	Mus musculus ribosomal protein L13a (RPL13A), mRNA.
7	Mus musculus calnexin (CANX), mRNA.
8	Mus musculus cytochrome c-1 (CYC1), mRNA.
9	Mus musculus succinate dehydrogenase complex, subunit A (SDHA), mRNA.
10	Mus musculus 18S rRNA gene
11	Mus musculus eukaryotic translation initiation factor 4A2 (EIF4A2), mRNA.
12	Mus musculus ATP synthase subunit (ATP5B), mRNA.

Real-time PCR was performed following the PrimerDesign geNorm SYBRgreen protocol (PrimerDesign Ltd., Southampton, Hampshire UK). Ct values

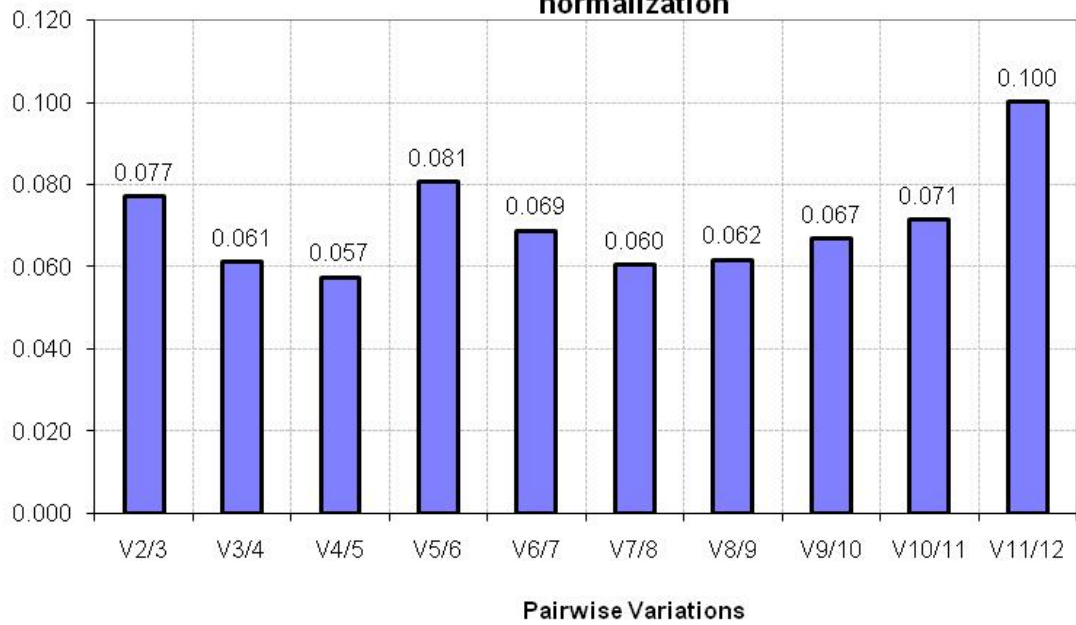
were converted into relative quantification data using the deltaCT method and prepared for input into the geNorm for Windows VBA applet for Microsoft Excel 2000/XP/2003 (version3.5), available for download at <http://medgen.ugent.be/~jvdesomp/genorm/>. The manufacturer's protocol was followed to analyze data using the software.

The first graph that was generated entitled average expression stability values of remaining control genes indicated the average expression stability value M of reference genes, starting from the least stable gene at the left, increasing expression stability ending with the two most stable genes on the right. Thus, the conclusion was reached that CANX and CYC1 are the two most stable genes among our developmental mouse brain RNA samples. The second graph generated entitled determination of the optimal number of control genes for normalization illustrated levels of variation in average reference gene stability with the addition of each reference gene to the equation. The graph shows the two most stably expressed genes on the left, including a third, fourth, and fifth gene etc. at each data point moving to the right. This is the pairwise variation V . PrimerDesign protocol (PrimerDesign Ltd.) recommends a V score below 0.15 as an ideal normalization. Among our samples, 0.077 is the V score using two normalizing genes, which will give ideal data. Therefore, these analyses lead to the selection of CANX and CYC1 for the normalization of RNA from mouse brain along the developmental set in real-time analysis.

Average expression stability values of remaining control genes



Determination of the optimal number of control genes for normalization



Appendix B

INSTITUTIONAL ANIMAL CARE AND USE COMMITTEE APPROVAL



Institutional Animal Care and Use Committee

MEMORANDUM

DATE: September 9, 2010

TO: **Grace M. Hobson, Ph.D.**

FROM: Paul T. Fawcett, Ph.D.

SUBJECT: "Mouse model of PMD due to duplication of PLP1" NBR-2007-007

The Institutional Animal Care and Use Committee (IACUC) have reviewed the above referenced protocol for approval, and the following decision has been made:

Action: Renewal approved

Date of Action: September 9, 2010

Approval Period: September 9, 2010 – September 8, 2011

Protocol Approval Number: NBR-2007-007

Approved Number of Animals:

Mus – mixed background (C57BL/6J and 129sv/ev) Yearly No. -199; Project Total -596

Mus – C57BL/6J Yearly No. - 233; Project Total -700

Please submit your Biosafety Classification form electronically to the Alfred I. duPont Hospital for Children Institutional Biosafety Committee via the link:

<http://www.nemours.org/research/committee/ibc.html>

Please note that the study cannot begin until the Office of Regulatory Compliance in Research Administration has received all approvals.

Please maintain this approval with your project records. A tally of the number of animals approved and the number ordered for the project will be maintained in the Life Science Center. If changes occur in your protocol or if you require more animals than approved, and amendment to your protocol will need to be submitted for consideration

If you have any questions regarding this memorandum, please contact Paul T. Fawcett, Ph.D. at x 6776 or email: pfawcett@nemours.org.

References

- Adams, D. J., Biggs, P. J., Cox, T., Davies, R., van der Weyden, L., Jonkers, J., Bradley, A. (2004). Mutagenic insertion and chromosome engineering resource (MICER). *Nature Genetics*, 36(8), 867-871.
- Anderson, T. J., Klugmann, M., Thomson, C. E., Schneider, A., Readhead, C., Nave, K. A., & Griffiths, I. R. (1999). Distinct phenotypes associated with increasing dosage of the PLP gene: Implications for CMT1A due to PMP22 gene duplication. *Annals of the New York Academy of Sciences*, 883, 234-246.
- Anderson, T. J., Schneider, A., Barrie, J. A., Klugmann, M., McCulloch, M. C., Kirkham, D., Griffiths, I. R. (1998). Late-onset neurodegeneration in mice with increased dosage of the proteolipid protein gene. *The Journal of Comparative Neurology*, 394(4), 506-519.
- Arroyo, E. J., Xu, T., Poliak, S., Watson, M., Peles, E., & Scherer, S. S. (2001). Internodal specializations of myelinated axons in the central nervous system. *Cell and Tissue Research*, 305(1), 53-66.
- Bauer, J., Bradl, M., Klein, M., Leisser, M., Deckwerth, T. L., Wekerle, H., & Lassmann, H. (2002). Endoplasmic reticulum stress in PLP-overexpressing transgenic rats: Gray matter oligodendrocytes are more vulnerable than white matter oligodendrocytes. *Journal of Neuropathology and Experimental Neurology*, 61(1), 12-22.
- Baumann, N., & Pham-Dinh, D. (2001). Biology of oligodendrocyte and myelin in the mammalian central nervous system. *Physiological Reviews*, 81(2), 871-927.
- Boggs, J. M. (2006). Myelin basic protein: A multifunctional protein. *Cellular and Molecular Life Sciences*, 63(17), 1945-1961.

- Bradl, M., Bauer, J., Inomata, T., Zielasek, J., Nave, K. A., Toyka, K., Wekerle, H. (1999). Transgenic lewis rats overexpressing the proteolipid protein gene: Myelin degeneration and its effect on T cell-mediated experimental autoimmune encephalomyelitis. *Acta Neuropathologica*, 97(6), 595-606.
- Brady, S. T., Witt, A. S., Kirkpatrick, L. L., de Waegh, S. M., Readhead, C., Tu, P. H., & Lee, V. M. (1999). Formation of compact myelin is required for maturation of the axonal cytoskeleton. *The Journal of Neuroscience*, 19(17), 7278-7288.
- Caro, P. A., & Marks, H. G. (1990). Magnetic resonance imaging and computed tomography in Pelizaeus-Merzbacher Disease. *Magnetic Resonance Imaging*, 8(6), 791-796.
- Cheon, J. E., Kim, I. O., Hwang, Y. S., Kim, K. J., Wang, K. C., Cho, B. K., Yeon, K. M. (2002). Leukodystrophy in children: A pictorial review of MR imaging features. *Radiographics*, 22(3), 461-476.
- Costantino-Ceccarini, E., & Morell, P. (1972). Biosynthesis of brain sphingolipids and myelin accumulation in the mouse. *Lipids*, 7(10), 656-659.
- Dobrina, A., Pausa, M., Fischetti, F., Bulla, R., Vecile, E., Ferrero, E., Tedesco, F. (2002). Cytolytically inactive terminal complement complex causes transendothelial migration of polymorphonuclear leukocytes in vitro and in vivo. *Blood*, 99(1), 185-192.
- Dubois-Dalcq, M., Behar, T., Hudson, L., & Lazzarini, R. A. (1986). Emergence of three myelin proteins in oligodendrocytes cultured without neurons. *The Journal of Cell Biology*, 102(2), 384-392.
- Edwards, A. M., Ross, N. W., Ulmer, J. B., & Braun, P. E. (1989). Interaction of myelin basic protein and proteolipid protein. *Journal of Neuroscience Research*, 22(1), 97-102.
- Ellis, D., & Malcolm, S. (1994). Proteolipid protein gene dosage effect in Pelizaeus-Merzbacher Disease. *Nature Genetics*, 6(4), 333-334.

- Fitzner, D., Schneider, A., Kippert, A., Mobius, W., Willig, K. I., Hell, S. W., Simons, M. (2006). Myelin basic protein-dependent plasma membrane reorganization in the formation of myelin. *The EMBO Journal*, 25(21), 5037-5048.
- Fujimoto, K., Roots, B. I., Burton, R. M., & Agrawal, H. C. (1976). Morphological and biochemical characterization of light and heavy myelin isolated from developing rat brain. *Biochimica Et Biophysica Acta*, 426(4), 659-668.
- Garbern, J. Y. (2007). Pelizaeus-Merzbacher Disease: Genetic and cellular pathogenesis. *Cellular and Molecular Life Sciences*, 64(1), 50-65.
- Garbern, J. Y., Yool, D. A., Moore, G. J., Wilds, I. B., Faulk, M. W., Klugmann, M., Griffiths, I. R. (2002). Patients lacking the major CNS myelin protein, proteolipid protein 1, develop length-dependent axonal degeneration in the absence of demyelination and inflammation. *Brain*, 125(Pt 3), 551-561.
- Gencic, S., Abuelo, D., Ambler, M., & Hudson, L. D. (1989). Pelizaeus-Merzbacher Disease: An X-linked neurologic disorder of myelin metabolism with a novel mutation in the gene encoding proteolipid protein. *American Journal of Human Genetics*, 45(3), 435-442.
- Gow, A., & Lazzarini, R. A. (1996). A cellular mechanism governing the severity of Pelizaeus-Merzbacher Disease. *Nature Genetics*, 13(4), 422-428.
- Griffiths, I., Klugmann, M., Anderson, T., Yool, D., Thomson, C., Schwab, M. H., Nave, K. A. (1998). Axonal swellings and degeneration in mice lacking the major proteolipid of myelin. *Science*, 280(5369), 1610-1613.
- Griffiths, I. R., Montague, P., & Dickinson, P. (1995). The proteolipid protein gene. *Neuropathology and Applied Neurobiology*, 21(2), 85-96.
- Hudson, L. D. (2003). Pelizaeus-Merzbacher Disease and spastic paraplegia type 2: Two faces of myelin loss from mutations in the same gene. *Journal of Child Neurology*, 18(9), 616-624.

- Hudson, L. D., Puckett, C., Berndt, J., Chan, J., & Gencic, S. (1989). Mutation of the proteolipid protein gene PLP in a human X chromosome-linked myelin disorder. *Proceedings of the National Academy of Sciences of the United States of America*, 86(20), 8128-8131.
- Huxley, A. F., & Stampfli, R. (1949). Evidence for saltatory conduction in peripheral myelinated nerve fibres. *The Journal of Physiology*, 108(3), 315-339.
- Inoue, K., Osaka, H., Imaizumi, K., Nezu, A., Takanashi, J., Arii, J., Lupski, J. R. (1999). Proteolipid protein gene duplications causing Pelizaeus-Merzbacher Disease: Molecular mechanism and phenotypic manifestations. *Annals of Neurology*, 45(5), 624-632.
- Inoue, K., Osaka, H., Sugiyama, N., Kawanishi, C., Onishi, H., Nezu, A., Kosaka, K. (1996). A duplicated PLP gene causing Pelizaeus-Merzbacher Disease detected by comparative multiplex PCR. *American Journal of Human Genetics*, 59(1), 32-39.
- Inoue, Y., Kagawa, T., Matsumura, Y., Ikenaka, K., & Mikoshiba, K. (1996). Cell death of oligodendrocytes or demyelination induced by overexpression of proteolipid protein depending on expressed gene dosage. *Neuroscience Research*, 25(2), 161-172.
- Kagawa, T., Ikenaka, K., Inoue, Y., Kuriyama, S., Tsujii, T., Nakao, J., Mikoshiba, K. (1994). Glial cell degeneration and hypomyelination caused by overexpression of myelin proteolipid protein gene. *Neuron*, 13(2), 427-442.
- Kanfer, J., Parenty, M., Goujet-Zalc, C., Monge, M., Bernier, L., Campagnoni, A. T., Zalc, B. (1989). Developmental expression of myelin proteolipid, basic protein, and 2',3'-cyclic nucleotide 3'-phosphodiesterase transcripts in different rat brain regions. *Journal of Molecular Neuroscience*, 1(1), 39-46.
- Karim, S. A., Barrie, J. A., McCulloch, M. C., Montague, P., Edgar, J. M., Iden, D. L., McLaughlin, M. (2010). PLP1 expression and turnover in a transgenic mouse model of Pelizaeus-Merzbacher Disease. *Glia*, 58(14), 1727-1738.

- Karim, S. A., Barrie, J. A., McCulloch, M. C., Montague, P., Edgar, J. M., Kirkham, D., McLaughlin, M. (2007). PLP overexpression perturbs myelin protein composition and myelination in a mouse model of Pelizaeus-Merzbacher Disease. *Glia*, 55(4), 341-351.
- Koeppen, A. H., & Robitaille, Y. (2002). Pelizaeus-Merzbacher Disease. *Journal of Neuropathology and Experimental Neurology*, 61(9), 747-759.
- Koeppen, A. H., Ronca, N. A., Greenfield, E. A., & Hans, M. B. (1987). Defective biosynthesis of proteolipid protein in Pelizaeus-Merzbacher Disease. *Annals of Neurology*, 21(2), 159-170.
- Li, Z., Yu, T., Morishima, M., Pao, A., LaDuca, J., Conroy, J., Yu, Y. E. (2007). Duplication of the entire 22.9 mb human chromosome 21 syntenic region on mouse chromosome 16 causes cardiovascular and gastrointestinal abnormalities. *Human Molecular Genetics*, 16(11), 1359-1366.
- McLaughlin, M., Barrie, J. A., Karim, S., Montague, P., Edgar, J. M., Kirkham, D., Griffiths, I. R. (2006). Processing of PLP in a model of Pelizaeus-Merzbacher Disease/SPG2 due to the rumpshaker mutation. *Glia*, 53(7), 715-722.
- Merzbacher, L. (1910) Eine eigenartige familiär-hereditäre Erkrankungsform (Aplasia axialis extra-corticalis congenita). *Z Gesamte Neurol Psychiatr.* 3, 1–138.
- Meusser, B., Hirsch, C., Jarosch, E., & Sommer, T. (2005). ERAD: The long road to destruction. *Nature Cell Biology*, 7(8), 766-772.
- Monge, M., Kadiiski, D., Jacque, C. M., & Zalc, B. (1986). Oligodendroglial expression and deposition of four major myelin constituents in the myelin sheath during development. an in vivo study. *Developmental Neuroscience*, 8(4), 222-235.
- Morello, D., Dautigny, A., Pham-Dinh, D., & Jolles, P. (1986). Myelin proteolipid protein (PLP and DM-20) transcripts are deleted in jimpy mutant mice. *The EMBO Journal*, 5(13), 3489-3493.

- Muncke, N., Wogatzky, B. S., Breuning, M., Sistermans, E. A., Endris, V., Ross, M., Rappold, G. (2004). Position effect on PLP1 may cause a subset of Pelizaeus-Merzbacher Disease symptoms. *Journal of Medical Genetics*, 41(12), e121.
- Nave, K. A., Bloom, F. E., & Milner, R. J. (1987). A single nucleotide difference in the gene for myelin proteolipid protein defines the jimpy mutation in mouse. *Journal of Neurochemistry*, 49(6), 1873-1877.
- Pelizaeus F. Über eine eigenthümliche Form Spastischer Lähmung mit Cerebralerschünungen auf hereditärer Grundlage (Multiple Sklerose). *Arch Psychiatr Nervenkr.* 1885;16:698-710
- Pfeiffer, S. E., Warrington, A. E., & Bansal, R. (1993). The oligodendrocyte and its many cellular processes. *Trends in Cell Biology*, 3(6), 191-197.
- Popot, J. L., Pham Dinh, D., & Dautigny, A. (1991). Major myelin proteolipid: The 4-alpha-helix topology. *The Journal of Membrane Biology*, 120(3), 233-246.
- Readhead, C., Schneider, A., Griffiths, I., & Nave, K. A. (1994). Premature arrest of myelin formation in transgenic mice with increased proteolipid protein gene dosage. *Neuron*, 12(3), 583-595.
- Regis, S., Grossi, S., Corsolini, F., Biancheri, R., & Filocamo, M. (2009). PLP1 gene duplication causes overexpression and alteration of the PLP1 splicing balance in fibroblasts from Pelizaeus-Merzbacher Disease patients. *Biochimica Et Biophysica Acta*, 1792(6), 548-554.
- Scherer, S. S., Vogelbacker, H. H., & Kamholz, J. (1992). Axons modulate the expression of proteolipid protein in the CNS. *Journal of Neuroscience Research*, 32(2), 138-148.
- Schneider, A., Lander, H., Schulz, G., Wolburg, H., Nave, K. A., Schulz, J. B., & Simons, M. (2005). Palmitoylation is a sorting determinant for transport to the myelin membrane. *Journal of Cell Science*, 118(Pt 11), 2415-2423.

- Seitelberger, F. (1954) Die Pelizaeus-Merzbachersche Krankheit. Klinisch-anatomische Untersuchungen zum Problem ihrer Stellung unter den diffusen Sklerosen. *Wien Z Nervenheilkd.* 9, 228–28
- Sheehan, D.C. and Hrapchak, B.B., 1980. *Theory and Practice of Histotechnology.* (pp. 46-48). St. Louis, MO: Mosby.
- Shirazi, Y., Rus, H. G., Macklin, W. B., & Shin, M. L. (1993). Enhanced degradation of messenger RNA encoding myelin proteins by terminal complement complexes in oligodendrocytes. *Journal of Immunology*, 150(10), 4581-4590.
- Simons, M., Kramer, E. M., Macchi, P., Rathke-Hartlieb, S., Trotter, J., Nave, K. A., & Schulz, J. B. (2002). Overexpression of the myelin proteolipid protein leads to accumulation of cholesterol and proteolipid protein in endosomes/lysosomes: Implications for Pelizaeus-Merzbacher Disease. *The Journal of Cell Biology*, 157(2), 327-336.
- Simons, M., Kramer, E. M., Thiele, C., Stoffel, W., & Trotter, J. (2000). Assembly of myelin by association of proteolipid protein with cholesterol- and galactosylceramide-rich membrane domains. *The Journal of Cell Biology*, 151(1), 143-154.
- Sistermans, E. A., de Coo, R. F., De Wijs, I. J., & Van Oost, B. A. (1998). Duplication of the proteolipid protein gene is the major cause of Pelizaeus-Merzbacher Disease. *Neurology*, 50(6), 1749-1754.
- Timsit, S., Martinez, S., Allinquant, B., Peyron, F., Puelles, L., & Zalc, B. (1995). Oligodendrocytes originate in a restricted zone of the embryonic ventral neural tube defined by DM-20 mRNA expression. *The Journal of Neuroscience*, 15(2), 1012-1024.
- Trofatter, J. A., Dlouhy, S. R., DeMyer, W., Conneally, P. M., & Hodes, M. E. (1989). Pelizaeus-Merzbacher Disease: Tight linkage to proteolipid protein gene exon variant. *Proceedings of the National Academy of Sciences of the United States of America*, 86(23), 9427-9430.

- van der Knaap, M. S., & Valk, J. (1989). The reflection of histology in MR imaging of Pelizaeus-Merzbacher Disease. *American Journal of Neuroradiology*, *10*(1), 99-103.
- Vandesompele, J., De Preter, K., Pattyn, F., Poppe, B., Van Roy, N., De Paepe, A., & Speleman, F. (2002). Accurate normalization of real-time quantitative RT-PCR data by geometric averaging of multiple internal control genes. *Genome Biology*, *3*(7),
- Verrier, J. D., Lau, P., Hudson, L., Murashov, A. K., Renne, R., & Notterpek, L. (2009). Peripheral myelin protein 22 is regulated post-transcriptionally by miRNA-29a. *Glia*, *57*(12), 1265-1279.
- Walz, K., Paylor, R., Yan, J., Bi, W., & Lupski, J. R. (2006). Rai1 duplication causes physical and behavioral phenotypes in a mouse model of dup(17)(p11.2p11.2). *The Journal of Clinical Investigation*, *116*(11), 3035-3041.
- Willard, H. F., & Riordan, J. R. (1985). Assignment of the gene for myelin proteolipid protein to the X chromosome: Implications for X-linked myelin disorders. *Science*, *230*(4728), 940-942.
- Wolf, N. I., Sistermans, E. A., Cundall, M., Hobson, G. M., Davis-Williams, A. P., Palmer, R., Woodward, K. J. (2005). Three or more copies of the proteolipid protein gene PLP1 cause severe Pelizaeus-Merzbacher Disease. *Brain*, *128*(Pt 4), 743-751.
- Wood, D. D., Vella, G. J., & Moscarello, M. A. (1984). Interaction between human myelin basic protein and lipophilin. *Neurochemical Research*, *9*(10), 1523-1531.
- Woodward, K., Kendall, E., Vetrie, D., & Malcolm, S. (1998). Pelizaeus-Merzbacher Disease: Identification of Xq22 proteolipid-protein duplications and characterization of breakpoints by interphase FISH. *American Journal of Human Genetics*, *63*(1), 207-217.

Woodward, K. J., Cundall, M., Sperle, K., Sistermans, E. A., Ross, M., Howell, G., Hobson, G. M. (2005). Heterogeneous duplications in patients with Pelizaeus-Merzbacher Disease suggest a mechanism of coupled homologous and nonhomologous recombination. *American Journal of Human Genetics*, 77(6), 966-987.

Yu, Y., & Bradley, A. (2001). Engineering chromosomal rearrangements in mice. *Nature Reviews Genetics*, 2(10), 780-790.